NeuroImage 207 (2020) 116404

Contents lists available at ScienceDirect

NeuroImage

journal homepage: www.elsevier.com/locate/neuroimage

Human subsystems of medial temporal lobes extend locally to amygdala nuclei and globally to an allostatic-interoceptive system

Adriana L. Ruiz-Rizzo [a,*], Florian Beissner [b], Kathrin Finke [a,c], Hermann J. Müller [a], Claus Zimmer [d], Lorenzo Pasquini [e,1], Christian Sorg [d,f,g,1]

[a] Department of General and Experimental Psychology, Ludwig-Maximilans-Universität München, Leopoldstraße 13, 80802, Munich, Germany
[b] Somatosensory and Autonomic Therapy Research, Institute for Diagnostic and Interventional Neuroradiology, Hannover Medical School, Carl-Neuberg-Straße 1, 30625, Hannover, Germany
[c] Hans-Berger-Klinik für Neurologie Universitätsklinikum Jena, Am Klinikum 1, 07747, Jena, Germany
[d] Department of Neuroradiology of Klinikum rechts der Isar, Technische Universität München, Ismaningerstraße 22, 81675, Munich, Germany
[e] Memory and Aging Center, Department of Neurology, University of California San Francisco, 675 Nelson Rising Lane, San Francisco, CA, 94158, USA
[f] TUM-Neuroimaging Center, Technische Universität München, Ismaningerstraße 22, 81675, Munich, Germany
[g] Psychiatry and Psychotherapy Klinikum rechts der Isar, Technische Universität München, Germany

ARTICLE INFO

Keywords:
Allostatic-interoceptive system
Amygdala
Intrinsic connectivity
Medial temporal lobe
Resting-state fMRI

ABSTRACT

In mammals, the hippocampus, entorhinal, perirhinal, and parahippocampal cortices (i.e., core regions of the human medial temporal lobes, MTL) are locally interlaced with the adjacent amygdala nuclei at the structural and functional levels. At the global brain level, the human MTL has been described as part of the default mode network and amygdala nuclei as parts of the salience network, with both networks collectively forming a large-scale brain system supporting allostatic-interoceptive functions. We hypothesized (i) that intrinsic functional connectivity of slow activity fluctuations would reveal human MTL subsystems locally extending to the amygdala; and (ii) that these extended local subsystems would be globally embedded in large-scale brain systems supporting allostatic-interoceptive functions. Capitalizing on resting-state fMRI data of three independent samples of cognitively healthy adults (one main and two replication samples: N = 101, 60, and 29, respectively), we analyzed the functional connectivity of fluctuating ongoing BOLD-activity within and outside the amygdala-MTL in a data-driven way using masked independent component and dual-regression analyses. We found that at the local level, MTL subsystems extend to the amygdala and are functionally organized along the longitudinal amygdala-MTL axis. These subsystems are characterized by consistent involvement of amygdala, hippocampus, and entorhinal cortex, but variable participation of perirhinal and parahippocampal regions. At the global level, amygdala-MTL subsystems selectively connect to salience, thalamic-brainstem, and default mode networks – the major cortical and subcortical components of the allostatic-interoceptive system. These findings provide evidence for integrated amygdala-MTL subsystems in humans, which are embedded within a larger allostatic-interoceptive system.

1. Introduction

The human medial temporal lobes (MTL) include the hippocampal, entorhinal, perirhinal, and parahippocampal cortices (Squire et al., 2004). An extensive body of research has focused on these core MTL regions' internal (i.e., local) and external (i.e., global) connectivity and how these regions underpin distinct cognitive functions including declarative memory or spatial navigation (e.g., Squire et al., 2004; Buzsaki and Moser, 2013; Strange et al., 2014). Specifically, distinct subsystems that are largely invariable across mammals have been identified within the core MTL (Strange et al., 2014). However, based on anatomy, structural connectivity, and functional interactions, these subsystems

Abbreviations: A-MTL, medial temporal lobes including amygdala; BOLD, blood oxygenation level-dependent signal; fMRI, functional magnetic resonance imaging; FWE, family wise error; ICA, independent component analysis; iFC, intrinsic functional connectivity; mICA, masked ICA; MTL, medial temporal lobes; rs-fMRI, resting state fMRI.

* Corresponding author. Ludwig-Maximilians-Universität München, Dept. of General and Experimental Psychology, Leopoldstr. 13, D-80802, Munich, Germany.
E-mail address: adriana.ruiz@lmu.de (A.L. Ruiz-Rizzo).

[1] These authors contributed equally to this work.

https://doi.org/10.1016/j.neuroimage.2019.116404
Received 27 September 2019; Accepted 25 November 2019
Available online 26 November 2019

consistently appear to extend beyond the core MTL, for example, to the amygdala nuclei. The current study used intrinsic connectivity of slowly fluctuating ongoing activity, to examine in humans for the presence of a 'local extension' of core MTL subsystems to the amygdala, and to explore the corresponding 'global extension' of the (extended) core MTL-amygdala subsystems to the rest of the brain.

At the local level, in rodents and non-human primates, core MTL regions are highly interrelated with adjacent amygdala nuclei in terms of anatomical proximity (Van Hoesen, 1995; Murray and Wise, 2004), structural connectivity (Pitkanen et al., 2000; Petrovich et al., 2001; Kemppainen et al., 2002), and functional interactions (Davis, 1992; Phelps, 2004; Gross and Canteras, 2012). Core MTL regions and the amygdala are anatomically adjacent in mammals (Insausti, 1993; McDonald, 1998), and, particularly in primates, are considered to be integral components of the MTL as a whole (Van Hoesen, 1995; Amunts et al., 2005). Concerning structural connectivity, dense reciprocal connections exist between the amygdala and core MTL regions (Saunders and Rosene, 1988). In the rat, for example, lateral, basal, and posterior cortical nuclei of the amygdala provide segregated, parallel, and point-to-point organized inputs to parahippocampal, entorhinal, and hippocampal cortices (Pitkanen et al., 2000; Petrovich et al., 2001; Kemppainen et al., 2002), and these topographically organized connections are highly conserved across species (Amaral and Insausti, 1992; Sah et al., 2003). Moreover, functional interaction takes place in a wide variety of functional domains, such as in fear-related unconditioned responses (Davis, 1992; Gross and Canteras, 2012), and emotional (Davis et al., 1994; Gross and Canteras, 2012; Tovote et al., 2015) or episodic memory (Kemppainen et al., 2002; Dolcos et al., 2004). Strong functional interactions between amygdala and core MTL regions are also evidenced by joint activity in response to novelty, conducive to successful information encoding (e.g., Sheth et al., 2008). For example, in humans, neurons in both hippocampus and amygdala increase their firing rate in response to novelty after a single trial (Rutishauser et al., 2006), and both hippocampus and amygdala respond to emotionally neutral visual stimuli that are novel in the context of a task (Blackford et al., 2010). Along with the hippocampus and amygdala, object novelty effects have also been observed in the parahippocampal gyrus, independently of environmental novelty effects (Kaplan et al., 2014). Similarly, evidence that sensory signals from the internal milieu can influence the activity of core MTL regions (e.g., Suarez et al., 2018), rather than only the activity of the amygdala (e.g., Lathe, 2001), also supports their close functional interrelatedness. Further, both hippocampus and amygdala might play a role in the pathophysiology of the autonomic and behavioral manifestations triggered by the production of pro-inflammatory cytokines that occurs during a period of infection (Dantzer et al., 2008).

In humans, intrinsic connectivity has been applied to study local subsystems across either amygdala nuclei or core MTL regions (e.g., Libby et al., 2012; Oler et al., 2012; Maass et al., 2015). Intrinsic connectivity is defined as functional connectivity (iFC) of ongoing slowly fluctuating brain activity (below 0.1 Hz), which is typically measured by correlated blood oxygenation levels of resting-state functional MRI (rs-fMRI) (Fox and Raichle, 2007; Smith et al., 2009). Regarding the amygdala, significant iFC has been found between the centromedial nuclei and the bed nucleus of the stria terminalis in both humans and macaques (Oler et al., 2012). Concerning the core regions of the MTL, an anterior-posterior iFC gradient has been found between the anterior-lateral entorhinal and perirhinal cortices and the proximal subiculum, as well as between the posterior-medial entorhinal and parahippocampal cortices and the distal subiculum (Maass et al., 2015). A comparable gradient-like local organization has also been reported for the hippocampus (e.g., Blessing et al., 2016).

At the global level in humans, iFC has also been applied to study intrinsic connectivity of amygdala nuclei or the core MTL to the rest of the brain (Kahn et al., 2008; Etkin et al., 2009; Roy et al., 2009; Ranganath and Ritchey, 2012; Navarro Schroder et al., 2015; Qin et al., 2015; Wang et al., 2016). For example, whereas basolateral amygdala nuclei link preferentially with the temporal and medial frontal cortices (the 'fronto-temporal' amygdala network; Etkin et al., 2009; Roy et al., 2009; Fox et al., 2015), the centromedial nuclei are functionally connected to the midbrain, thalamus, and cerebellum (Etkin et al., 2009). Similarly, the anterior-lateral entorhinal cortices connect with the medial-prefrontal and orbitofrontal cortices, whereas the posterior-medial entorhinal cortices are preferentially connected with posterior parietal areas (Navarro Schroder et al., 2015). Comparable distinct global iFC patterns have also been described for the hippocampus (Kahn et al., 2008; Robinson et al., 2015). At the large-scale system level, the amygdala and the core MTL have been respectively described as part of the salience network – which also includes the insula, the anterior cingulate, and the hypothalamus (e.g., Seeley et al., 2007) – and the default mode network – comprising the precuneus, posterior cingulate, angular gyrus, and medial prefrontal cortex (e.g., Buckner et al., 2008). Recently, both networks have been suggested to be part of a large-scale brain system that appears to support distinct functional domains (i.e., emotion, memory, and social cognition) and is thought to link the control of homeostatic body-focused (i.e., interoceptive) processes with the control of interactions with the environment (i.e., allostatic; Barrett and Simmons, 2015; Kleckner et al., 2017). Beyond the salience and default mode networks, this allostatic-interoceptive system includes key subcortical regions such as parts of striatum, pallidum, thalamus, hypothalamus, and upper brainstem.

On this background, the current study examined for a local and a global extension of the core MTL to the amygdala (i.e., 'A-MTL') in humans, as defined by iFC. At the local level, based on structural connectivity evidence of A-MTL subsystems in rodents and primates, we expected analogous subsystems characterized by iFC to consistently span core regions of the MTL *and* the amygdala. At the global level, based on the respective iFC patterns of the core MTL and the amygdala with networks contributing to the allostatic-interoceptive system, we expected that A-MTL subsystems collectively extend to the allostatic-interoceptive system through iFC. To test these hypotheses, we assessed 101 young healthy participants and analyzed the intrinsic connectivity of fluctuating ongoing rs-fMRI activity within and outside the A-MTL in a data-driven way using masked independent component analysis (Beissner et al., 2014; Blessing et al., 2016) and dual regression (Beckmann et al., 2009; Filippini et al., 2009). Specifically, our mask of independent component analysis was centered on the A-MTL to reveal A-MTL subsystems on the one hand, and their global extension on the other. To control the reliability of our findings, we replicated our approach in two further, non-overlapping samples.

2. Materials and methods

2.1. Participants

One hundred and one healthy young participants (age: 26.7 ± 0.7 years, range: 25–27, 41 females) underwent rs-fMRI at the Department of Neuroradiology, Klinikum rechts der Isar, Munich, Germany. The local ethics committee of the Klinikum rechts der Isar approved the study, and all participants gave written informed consent for their participation. Study exclusion criteria were current or past neurological and psychiatric disorders, as well as severe systemic diseases or neurotropic medication. The rs-fMRI data of two additional samples of cognitively normal adults participating in other studies (one from our group, and one from a public data base) were used for replication analyses (Replication sample 1: N = 60, age: 36.4 ± 13.6 years, range: 18–65, 18 females. Replication sample 2: N = 29, age: 26.0 ± 4.1 years, range: 18–35, 14 females; see Supplementary Material for more details).

2.2. MRI data acquisition

MRI data acquisition of the main sample was performed on a Philips Achieva 3T TX system (Netherlands), using an 8-channel SENSE head

coil. Functional MRI T2*-weighted data were collected for 10 min 52 s while participants were resting with eyes closed, and after being instructed not to fall asleep. We verified that subjects stayed awake by interrogating via intercom immediately after the rs-fMRI scanning run. Two hundred and fifty volumes of blood oxygenation level dependent (BOLD) rs-fMRI signal per individual were acquired using a gradient-echo echo planar imaging (GRE-EPI) sequence: Repetition time, TR = 2608 ms; echo time, TE = 35 ms; phase encoding direction: anterior–posterior; flip angle = 90°; field of view, FOV = 230 mm; matrix size = 64 × 64, 41 interleaved slices, and no interslice gap; reconstructed voxel size = 3.59 mm isotropic. Subsequently, a high-resolution T1-weighted image was acquired using a 3D-MPRAGE sequence with the following parameters: TR = 7.7 ms; TE = 3.9 ms; inversion time, TI = 1300 ms; flip angle = 15°; 180 sagittal slices, reconstruction matrix: 256 × 256; reconstructed voxel size 1 mm isotropic.

2.3. Data preprocessing

Functional MRI data were preprocessed using the Data Processing Assistant for Resting-State fMRI toolbox (DPARSF; Chao-Gan and Yu-Feng, 2010) and SPM12 (http://www.fil.ion.ucl.ac.uk/spm). After discarding the first 5 rs-fMRI volumes to avoid magnetization effects, functional volumes were realigned to correct for head motion. Each participant's T1-weighted structural image was segmented into gray matter (GM), white matter (WM), and cerebrospinal fluid (CSF) using the tissue classification algorithm implemented in SPM, which is based on prior probabilities of voxels belonging to each tissue type (obtained from scans of 152 healthy young subjects provided by the Montreal Neurological Institute, MNI). Each participant's rs-fMRI volumes were co-registered to their high-resolution structural T1 image by using boundary-based registration, and then transformed to MNI space at 2 × 2 × 2-mm^3 resolution using nonlinear registration derived from the T1-image normalization and then spatially smoothed using a 5 mm full-width-at-half-maximum (FWHM) Gaussian kernel. To control for movement artifacts, we used as criterion peak-to-peak motion below 1 mm or 1° in any direction. Based on this criterion, all subjects were included in further analyses. To control for nuisance covariates, we extracted the mean time series for WM and CSF from the rs-fMRI data. Each individual's segmented high-resolution structural MRI was used to calculate WM and CSF specific mean time series, with tissue type probability of 0.8, by averaging across all voxels within the tissue masks. WM, CSF, and global signals, and six head motion parameters (three translations, three rotations) for each subject were regressed out from the rs-fMRI data.

2.4. Data analysis

We analyzed the preprocessed rs-fMRI data by employing masked independent component analysis (mICA) combined with dual-regression analysis (Beissner et al., 2014; Blessing et al., 2016). Masked ICA localized iFC-based sources within a mask (i.e., the local A-MTL subsystems), whereas whole-brain dual regression identified corresponding global-iFC patterns related to the local sources. A mask of the A-MTL was built by combining the bilateral masks of the amygdala, hippocampus, and entorhinal, perirhinal, and posterior parahippocampal cortices, derived from the Harvard-Oxford cortical and subcortical probabilistic structural atlases and the Jülich histological atlas, using Fslview (http://fsl.fmrib.ox.ac.uk/fsl/fslview/). These masks were added up using the Imcalc toolbox of SPM (http://www.fil.ion.ucl.ac.uk/spm/), binarized at a threshold probability of 0.5, and resampled to the size of our functional data. Next, the preprocessed rs-fMRI data were temporally concatenated and analyzed by probabilistic ICA (Beckmann and Smith, 2004) restricted to the A-MTL mask, using the FSL *melodic* command (http://www.fmrib.ox.ac.uk/fsl/). First, these data were normalized for voxel-wise mean and variance, and then reduced into a 20-dimensional subspace by probabilistic principal component analysis. A dimensionality of 20 was chosen based on a series of control analyses, which are described in detail below. Subsequently, data were decomposed into time courses and spatial maps by optimizing for non-Gaussian spatial distributions using a fixed-point iteration technique (Hyvarinen, 1999). The resulting group-level component maps are divided by the standard deviation of the residual noise and thresholded by fitting a mixture model to the histogram of intensity (Beckmann and Smith, 2004).

2.5. Dual regression

To assess both local- and global-iFC of A-MTL subsystems, dual-regression analyses were conducted (Beckmann et al., 2009; Filippini et al., 2009; Smith et al., 2014; Nickerson et al., 2017). Dual regression is a multivariate approach that allows the estimation of an *individual* version of the group-level spatial maps. Dual regression works in two steps. In the first step, the set of spatial independent components derived by group-level mICA is regressed on the individual participant's 4D dataset in a multiple regression. This results in a set of participant-specific time courses, one per group-level spatial map. In the second step, those time courses are regressed in a second multiple regression, on the same 4D dataset, resulting in participant-specific spatial maps, one per group-level spatial map. Participant-specific spatial maps were further analyzed in two ways: (i) maps were restricted to the A-MTL mask and used to estimate local-iFC patterns and iFC peaks of A-MTL; (ii) a whole-brain mask was used to estimate the global-iFC patterns that correspond to those local-iFC patterns. Next, the statistical significance of both restricted and unrestricted maps was assessed in a two-sided one-sample *t*-test using FSL's *randomise* permutation-testing tool, resulting in *t*- and *p*-value maps for each component involved in the analysis. Specifically, the results were based on 500 permutations and a p-value of 0.05, corrected for multiple comparisons by threshold-free cluster enhancement (Smith and Nichols, 2009).

2.6. Separation of neural from non-neural local-iFC patterns

To separate local-iFC patterns of 'neural' and 'non-neural' origin, we analyzed their associated global-iFC patterns to compute, for each one of them, the percentage of voxels that lay on GM, WM, and CSF. We used the tissue probability maps of the three tissue types of interest (downloaded from: https://www.fil.ion.ucl.ac.uk/spm/toolbox/TPM/) (Blaiotta et al., 2018). The thresholded (to a probability of 0.9) maps were multiplied with the thresholded (voxels greater than 0.95) and binarized p-value maps of our mICA independent components (following Beissner et al., 2014). From this multiplication, we obtained, for each global-iFC pattern, the number of voxels present in each tissue type (i.e., GM, WM, and CSF). Finally, we calculated, for each global-iFC pattern, the percentage of voxels in CSF with respect to the total number of voxels (i.e., in the three tissue types; based on the approach of Beissner et al., 2014). Based on the mean percentage of voxels in CSF (from all global-iFC patterns), we tagged as 'non-neural' those global-iFC patterns with a percentage at or above the mean and as 'neural' those below the mean (see Table S1). Our results are thus based only on those iFC patterns classified as 'neural.'

2.7. Anatomical characterization of local-iFC patterns

After excluding non-neural local-iFC patterns, we characterized the remaining maps anatomically. Specifically, the iFC peaks of these maps were identified using the FSL tool *fslstats*. Peaks were classified as anterior (y = 4 to −18 mm), middle (y = −19 to −31 mm), or posterior (y = −32 to −42 mm) [following the classification of the longitudinal axis of whole MTL by Kivisaari et al. (2013)]. To further quantify the relative contribution of each A-MTL structure, we calculated the effect size (Cohen's *d*) of each structure within each local-iFC pattern. For this, we

used the *t*-maps generated from the local dual regression. For values > 0, we computed the mean and standard deviation of the local-iFC pattern's *t*-map. Next, we computed each structure's mean *t*-value for each local-iFC pattern. Finally, we subtracted the local-iFC pattern's mean *t*-value from the mean *t*-value of each structure and divided the result by the local-iFC pattern's *t*-value standard deviation. The extent of iFC (i.e., involvement of each A-MTL structure) was also examined for each map and slice by slice in the coronal plane.

2.8. Network characterization of global-iFC patterns

Based on previous findings relating local-iFC subsystems of core MTL regions and amygdala to known large-scale brain networks (Kahn et al., 2008; Etkin et al., 2009; Roy et al., 2009; Ranganath and Ritchey, 2012; Navarro Schroder et al., 2015; Qin et al., 2015; Wang et al., 2016), we expected that the global-iFC of A-MTL subsystems would also be embedded in the functional architecture of large-scale brain networks (Allen et al., 2011; Yeo et al., 2011; Raichle, 2015) – particularly those constituting the allostatic-interoceptive system, i.e., the default mode, salience, and brainstem-thalamus networks. Thus, we compared the global-iFC patterns of the 'neural' local-iFC patterns with templates of large-scale brain networks derived from a study that estimated these networks from rs-fMRI data of about 600 healthy participants (Allen et al., 2011). We calculated spatial cross-correlation coefficients between those templates and our global-iFC patterns using the *fslcc command* (https://fsl.fmrib.ox.ac.uk/fsl/fslwiki/Fslutils) in FSL (Jenkinson et al., 2012). In short, this command calculates the covariance across all spatial dimensions (x, y, and z), for each volume, between two 4D images. Based on this covariance, as well as on the multiplication of the volume-wise standard deviations, it computes the correlation coefficient between each pair of volumes of both images. The result thus reflects the spatial overlap (across voxels) between components. The global-iFC pattern with the highest cross-correlation coefficient was chosen as the pattern best matching a particular known large-scale brain network.

2.9. Control analyses: number of ICA dimensions, replication, signal-to-noise ratio, and smoothing

Since ICA results depend heavily on the number of dimensions used to decompose the data, we searched for the optimal dimensionality in our specific A-MTL mICA approach, given the characteristics of our data (i.e., TR, number of volumes, or data sets). Specifically, we performed a series of control analyses of three ICA dimensionalities, 10, 20, and 30. We defined the 'optimal dimensionality' based on the neural global-iFC patterns, whereby 'optimal' meant that the global-iFC patterns were separated into a maximum number without generating qualitatively new iFC-patterns, but also without generating redundant iFC patterns.

Second, to control both the reliability of our findings and the impact of smaller sample size, we replicated our approach in two further independent samples. We used control samples with lower sample sizes (one medium sized and one small sized) compared to that used in the present study (replication sample 1: N = 60; replication sample 2: N = 29). Moreover, the size of one of the samples approached more closely the sample size typically used in patient studies (i.e., ~30). Both replication datasets have been previously described and used for other analyses (see Supplementary Material for details). Using as well the optimal mICA dimensionality and selection of the local-iFC patterns via global-iFC patterns, we then tested their respective cross-correlations with the original results, as described in more detail in the Supplementary Material.

Finally, given the relatively small size of the A-MTL structures and their ventromedial location, there could be differences in magnetic susceptibility. Moreover, the spatial blurring or smoothing performed during preprocessing might compromise the spatial specificity of our results. Thus, first, to assess the impact of possible differences in magnetic susceptibility across A-MTL structures, we calculated the temporal signal-to-noise ratio. Second, to assess the possible impact of the smoothing step applied during data preprocessing, we additionally obtained local-iFC patterns from unsmoothed data (see Supplementary Material for details).

3. Results

3.1. A-MTL global-iFC patterns: 'neural origin' and optimal number of dimensions for mICA, anatomy-based naming, and correspondence with large-scale functional networks

First, for 10-, 20-, and 30-dimension mICA, we defined 'neural' and 'non-neural' global-iFC patterns (see Fig. 1 and Table S1 for an example). Based on a group mean of 14.6 ± 5.9% of global-iFC pattern voxels in CSF, 5 iFC patterns were selected as 'neural,' and five as 'non-neural' in the mICA with 10 components. For the mICA with 20 components, 12 were selected as neural and 8 as non-neural based on a group mean of 14.1 ± 8.4% of global-iFC pattern voxels in CSF. Finally, for the mICA with 30 components, 14 were identified as neural and 16 as non-neural, based on a group mean of 13.1 ± 5.7% of global-iFC pattern voxels in CSF.

Second, we defined the mICA-dimensionality that could represent an optimal solution to reduce our data (Fig. S1 and Tables S2 and S3). We selected a dimensionality of 20 as optimal for the mICA because neural global-iFC patterns tended to merge in the 10-dimension mICA, but to split (without providing new information) or repeat in the 30-dimension mICA (Table S2). For example, a global-iFC pattern involving frontal and parietal cortices in 10-mICA (Fig. S1) could be split into three global-iFC patterns in 20-mICA, with two involving lateral parietal cortices and one involving medial frontal and parietal cortices. These three global-iFC patterns could, in turn, also appear in the 30-mICA but with additional redundant or uninformative iFC patterns (see also Table S2 and Table S3). However, overall, all 'neural' patterns were found in all three dimensionalities, indicating that our results are relatively independent of the number of components chosen. Moreover, in the 20-dimension mICA, neural and non-neural patterns did not differ in the average percentage of coverage of the A-MTL, indicating that our results do not depend on the particular number of neural patterns identified (Table S4). Fig. 1 shows the twelve local-iFC patterns and their corresponding global-iFC patterns identified as of 'neural' origin (A), which are the basis for the following results; additionally, the 8 local- and global-iFC patterns rated as 'non-neural' (B) for the mICA with dimensionality of 20 are shown.

We named A-MTL global-iFC patterns according to the regions they included, as a way to identify them without implying any a priori function (Fig. 1 and last column of Table 1). For example, we labelled those containing overlapping regions based on their laterality or dorsal or ventral predominance: "parietal right [IC1]", "ventral parietal [IC8]", "parietal left [IC10]", or "dorsal parietal [IC18]", respectively.

These A-MTL global-iFC patterns comprised regions of and corresponded well to large-scale brain networks reported in the literature (Table 2). For example, one of our global-iFC patterns (i.e., IC15 – Frontoinsular) corresponded to the "salience network" of Allen et al. (2011), one (i.e., IC2 – Thalamus + basal ganglia) to "basal ganglia," and at least seven of our global-iFC patterns (e.g., IC12/IC5 – Ventral/Dorsal frontal and parietal or IC8/IC18 – Ventral/Dorsal parietal) to the "DMN posterior lateral."

3.2. A-MTL local-iFC patterns: localizing and naming, longitudinal organization, and consistent involvement of hippocampus, amygdala and entorhinal cortex for each pattern

Derived from the neural A-MTL global-iFC patterns, Figs. 2–4 represent the A-MTL local-iFC patterns: the patterns of main interest in the current study. In particular, Fig. 2A presents an overview of the neural iFC peak voxel location in the A-MTL for local-iFC patterns, based on the 20-dimension mICA output (see MNI coordinates in Table 1). Fig. 2B shows the relative contribution (i.e., the effect size) of each A-MTL

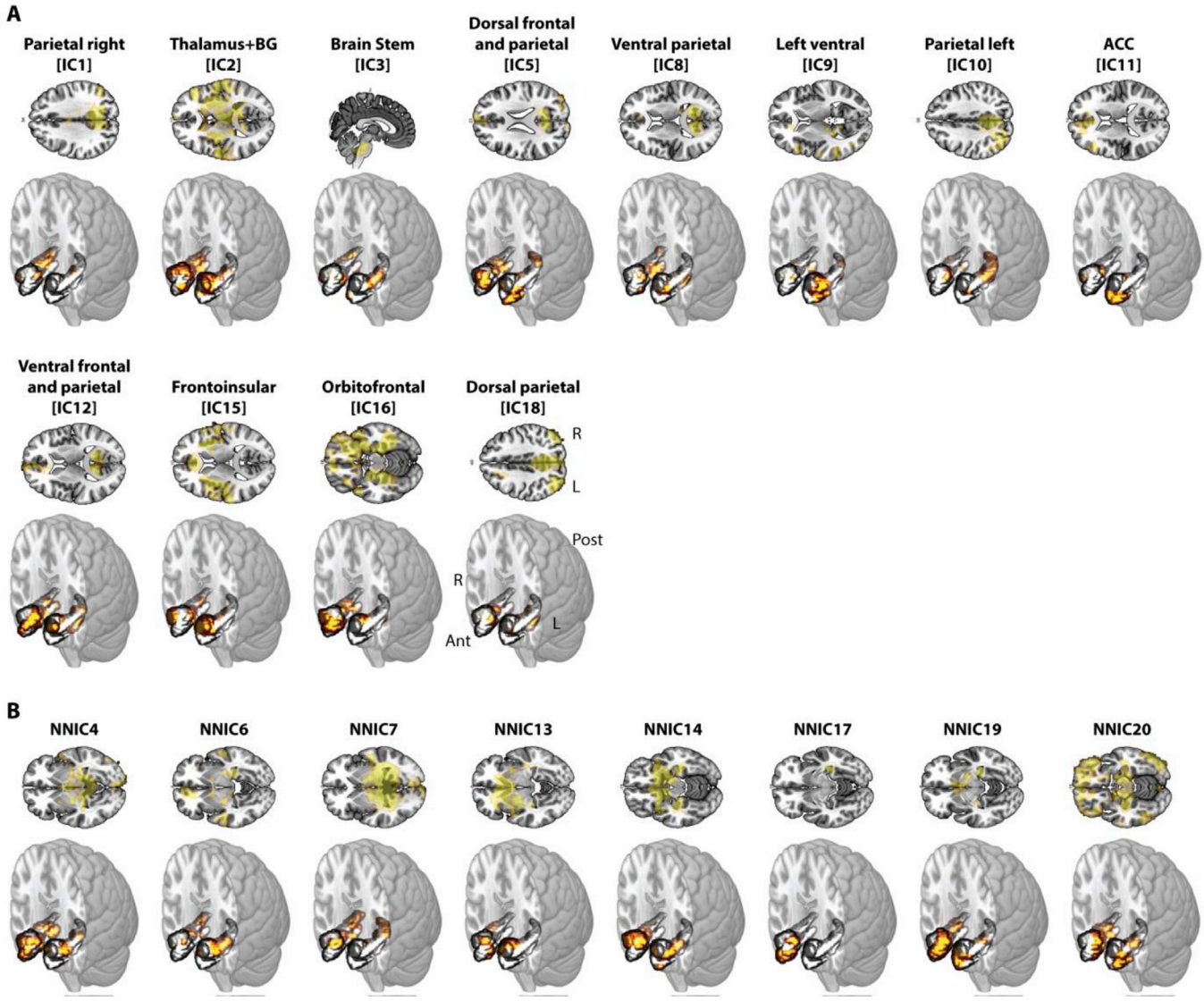

Fig. 1. A-MTL local- and global-iFC patterns. A-MTL iFC patterns identified as of 'neural' (A) or 'non-neural' (B) origin and obtained from the masked independent component analysis (mICA) with 20 dimensions and subsequent whole-brain dual regression. ACC: anterior cingulate cortex; BG: basal ganglia; IC: independent component; NN: non-neural.

structure across A-MTL local-iFC patterns. Each A-MTL structure contributed the most in a different A-MTL local-iFC pattern (the corresponding bar plot for the non-neural local-iFC patterns is shown in Supplementary Fig. S2). As peak voxels of local-iFC patterns refer to voxels with the maximum *t*-value in each local-iFC pattern, we used the peak voxel to inform us about the iFC "origin" or "anchor" of each local-iFC pattern. Similarly, as the relative contribution of each A-MTL structure was distinct for each local-iFC pattern, we used this information to label and more easily identify the neural local-iFC patterns (i.e., with "AM" if amygdala contributed the most to that pattern). The "Anterior," "Central," and "Posterior" preceding the local patterns' label indicate the relative location along the whole A-MTL (see section 2.7 for details).

Based on the iFC peak along the A-MTL longitudinal axis, we arranged the twelve identified neural A-MTL local-iFC patterns (Fig. 3 and Table 1). The predominance of each structure's contribution followed the longitudinal organization according to the peak location (Table 1) in almost all local-iFC patterns (two exceptions were the second and fifth patterns, for which the peaks were located in the Anterior HC, but the greatest effect sizes came from the entorhinal cortex-amygdala and amygdala, respectively). The peak (red voxels framed by a red square) location, as well as the extension (yellow voxels) along the entire A-MTL of each local-iFC pattern are plotted on coronal slices in Fig. 3.

After that, to visualize and analyze the spatial outline of the twelve identified A-MTL local-iFC patterns in more detail, we mapped each local-iFC pattern onto a longitudinally organized, slice-wise, rectangular schematic of the A-MTL with color-coded 'boxes' for amygdala, hippocampus, entorhinal, perirhinal, and parahippocampal cortices (Fig. 4, center). Every local-iFC pattern included the different A-MTL structures to different extents (different colors and different intensities on the black background of the schematics of Fig. 4). However, despite such differential involvement of A-MTL structures in the local-iFC patterns, three of those structures were always present (although to different degrees) in every local-iFC pattern, namely: the amygdala, the hippocampus, and the entorhinal cortex. This result indicates the consistent involvement of these three structures across the A-MTL local-iFC patterns. In contrast, the perirhinal and posterior parahippocampal cortices did not appear in all local-iFC patterns. Specifically, the perirhinal cortex (in red) was not present in the Central HC - 3 and Posterior PHC - 2 local iFC-patterns. Similarly, the posterior parahippocampal cortex did not appear in the Anterior AM-1.

Table 1
Local-iFC patterns organized along the A-MTL longitudinal axis based on the peak iFC and corresponding global-iFC patterns.

Coordinates (x, y, z) of the peak voxel in MNI space	A-MTL structure — iFC greatest effect size	A-MTL structure — iFC peak location	Brain structures of global-iFC patterns	Global-iFC pattern label
−26, **-4**, −16	Anterior AM	Anterior AM	Anterior cingulate cortex, lateral and medial orbitofrontal cortex, insular cortex, putamen, temporal pole, and supramarginal gyrus, ventral striatum, ventral pallidum, cerebellum (vermis), and periaqueductal gray	Frontoinsular (IC15)
26, **-6**, −24	Anterior EC-AM	Anterior HC	Postcentral gyrus, precuneus, occipital cortex, fusiform cortex, insula, bilateral orbitofrontal cortex, temporal pole	Orbitofrontal (IC16)
−24, **-8**, −36	Anterior PRC	Anterior PRC	Medial orbitofrontal cortex, fronto-insular cortex, temporal lobe, ventral striatum, and putamen	Anterior cingulate cortex (IC11)*
30, **-12**, −20	Anterior HC	Anterior HC	Brain stem, cerebellum, thalamus, middle temporal gyrus, insula, fusiform cortex, precentral gyrus, inferior lateral occipital cortex	Brain stem (IC3)
22, **-12**, −18	Anterior AM	Anterior HC	Insular cortex, superior temporal gyrus, nucleus accumbens, caudate nucleus, putamen, and thalamus	Thalamus + basal ganglia (IC2)
−26, **-14**, −18	Anterior HC	Anterior HC	Left orbitofrontal cortex, left inferior frontal gyrus, left superior and middle temporal gyrus, left thalamus, left caudate, left fusiform cortex, left lateral occipital cortex	Left ventral (IC9)
−20, **-16**, −18	Anterior HC	Anterior HC	Medial frontal cortex, ventromedial frontal cortex, subgenus anterior cingulate cortex, dorsomedial frontal cortex, middle temporal gyrus, retrosplenial cortex, precuneus, posterior cingulate cortex, nucleus accumbens, and lower brain stem	Ventral frontal and parietal (IC12)
34, **-20**, −14	Central HC	Central HC	Dorsomedial prefrontal cortex, ventromedial prefrontal cortex, anterior part of superior and middle temporal gyrus, nucleus accumbens, precuneus, posterior cingulate cortex, and occipital cortex	Dorsal frontal and parietal (IC5)
32, **-26**, −14	Central HC	Central HC	Right inferior parietal lobule and posterior cingulate cortex, bilateral precuneus and temporal lobe	Parietal right (IC1)
−26, **-28**, −14	Central HC	Central HC	Left inferior parietal lobule and posterior cingulate cortex, bilateral precuneus and temporal lobe	Parietal left (IC10)
20, **-32**, −14	Posterior PHC	Posterior PHC	Middle temporal gyrus, paracingulate gyrus, insula, fusiform cortex, inferior parietal lobule, precuneus, anterior cingulate cortex	Ventral parietal (IC8)
−24, **-32**, −18	Posterior PHC	Posterior PHC	Bilateral posterior parietal cortex, precuneus, posterior cingulate cortex, hypothalamus, cerebellum, and brain stem	Dorsal parietal (IC18)

AM = amygdala; EC = entorhinal cortex; HC = hippocampus; iFC = intrinsic functional connectivity; IC = independent component; PHC = posterior parahippocampal cortex; PRC = perirhinal cortex. *It resembles the semantic appraisal network described in previous studies (Guo et al., 2013; Zhou and Seeley, 2014).

Table 2
Spatial cross-correlation between large-scale brain network templates and the current A-MTL global-iFC patterns.

Global-iFC patterns	Allen et al.'s (2011) networks
IC15 – Frontoinsular	IC55, "salience," r = 0.14
IC16 – Orbitofrontal	IC53, "DMN posterior lateral," r = 0.12
IC11 – Anterior cingulate cortex	IC25, "DMN anterior medial," r = 0.26
IC3 – Brain stem	IC42, "frontal," r = 0.11
IC2 – Thalamus + basal ganglia	IC21, "basal ganglia," r = 0.40
IC9 – Left ventral	IC67, "visual," r = 0.11
IC12 – Ventral frontal and parietal	IC53, "DMN posterior lateral," r = 0.28
IC5 – Dorsal frontal and parietal	IC53, "DMN posterior lateral," r = 0.20
IC1 – Parietal right	IC53, "DMN posterior lateral," r = 0.34
IC10 – Parietal left	IC53, "DMN posterior lateral," r = 0.33
IC8 – Ventral parietal	IC53, "DMN posterior lateral," r = 0.35
IC18 – Dorsal parietal	IC53, "DMN posterior lateral," r = 0.48

Global-iFC patterns with the highest cross-correlation coefficient with Allen et al.'s networks (2011), calculated with the *fslcc* command of FSL.

3.3. A-MTL global-iFC patterns revisited: longitudinal organization and its relationship to A-MTL local-iFC patterns

Next, we explored the A-MTL global-iFC patterns with respect to the longitudinal outline of the A-MTL local-iFC patterns. We found a longitudinal gradient for *global*-iFC patterns that remarkably corresponds to that of local-iFC peaks (Fig. 4, outer columns). In more detail, the most anterior (dorsal) global-iFC patterns – which covered frontoinsular, orbitofrontal, and anterior cingulate cortices, and resembled a frontal and the salience networks of Allen et al. (2011) (Table 2) – corresponded to the three most anterior local-iFC patterns with iFC peaks in the amygdala, anterior hippocampus, and perirhinal cortex, respectively. Subcortical (ventral) global-iFC patterns – which covered brainstem, basal ganglia, and thalamus and resembled the basal ganglia network of Allen et al. (Table 2) – corresponded to the next two anterior local-iFC patterns with two iFC peaks in the anterior hippocampus. Finally, the remaining seven global-iFC patterns corresponded to local-iFC patterns with two iFC peaks in the anterior hippocampus, three in the central hippocampus, and two in the posterior parahippocampal cortex. These

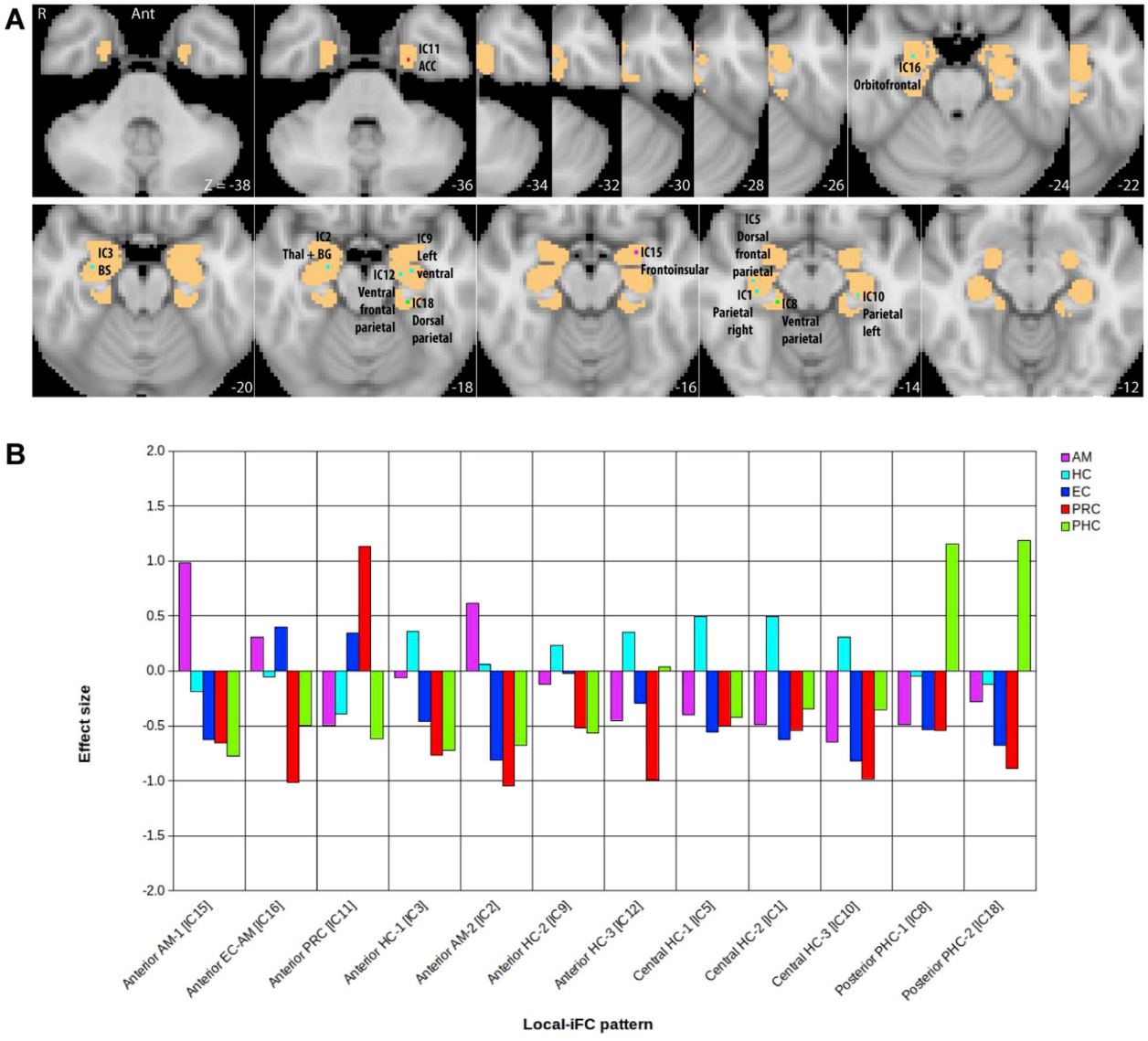

Fig. 2. Overview of iFC peaks (A) and effect sizes of A-MTL structures across 'neural' local-iFC patterns (B). (A) IFC peaks are overlaid onto the A-MTL mask in axial slices (MNI coordinates shown on the bottom right). Peaks' colors correspond to the structures labelled in B and peaks' names correspond to labels in Fig. 1 (B) Effect size calculated from the *t*-maps obtained from the dual regression (see text for details). ACC: anterior cingulate cortex; AM: amygdala; BG: basal ganglia; BS: brain stem; HC: hippocampus; EC: entorhinal cortex; PRC: perirhinal cortex; PHC: parahippocampal cortex; Thal: thalamus.

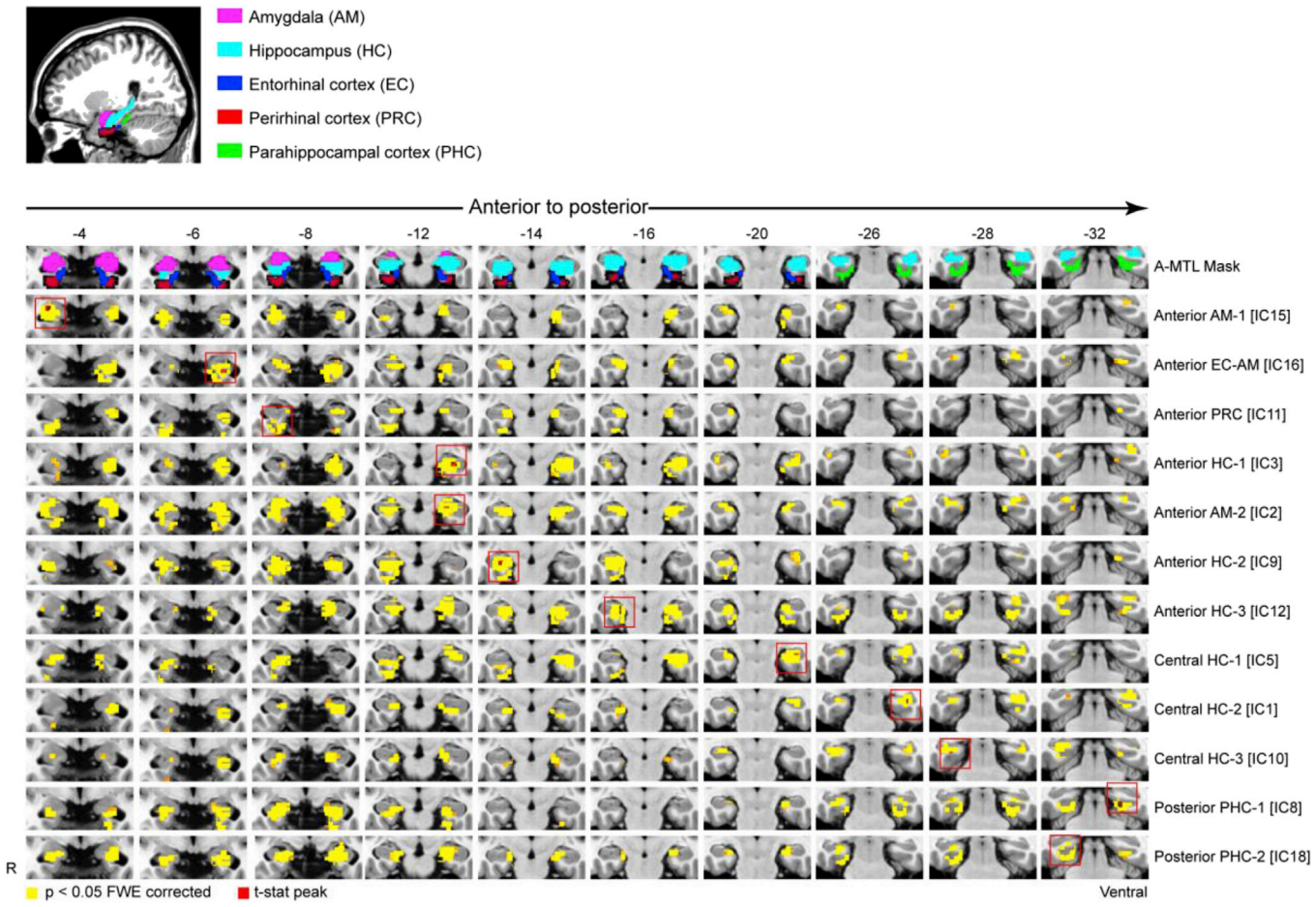

Fig. 3. Local-iFC patterns' peaks and extension. The peaks of the twelve 'neural' local-iFC patterns are shown across coronal slices (y-coordinate on the top) in red, on the patterns' extension (shown in yellow).

seven global-iFC patterns covered anterior and posterior cingulate, dorsal and ventral prefrontal, middle temporal, and inferior parietal cortices as well as lower brain stem, hypothalamus, and cerebellum, and resembled subparts of the default mode network (Table 2). Thus, the anatomical organization of A-MTL local-iFC patterns along the longitudinal axis resulted in a similar organization (i.e., anterior-posterior) of A-MTL global-iFC patterns, which match the salience network, default-mode networks as well as subcortical networks.

3.4. Control analyses: replicability, impact of smoothing and signal-to-noise ratio, and amygdala specificity

3.4.1. Reliability of A-MTL local- and global-iFC patterns

First, we tested the replicability of A-MTL subsystems. We found similar global-iFC patterns based on mICA restricted to the A-MTL mask in two different samples of cognitively normal adult participants (Figs. 5 and 6). In more detail, for the replication sample 1 (N = 60), 10 global-iFC patterns were identified as 'neural,' following the same approach used for the original sample. Of these 10, six had highest spatial cross-correlations with the original sample's global-iFC patterns: three had the highest spatial cross-correlation with each one of the original brain stem, ventral frontal and parietal, and parietal right; one had the highest cross-correlation with both the frontoinsular and thalamus/basal ganglia iFC patterns of the original sample; one had the highest cross-correlation with the original orbitofrontal and three parietal; and one had the highest cross-correlation with the original anterior cingulate and left ventral global-iFC patterns (mean coefficient of spatial cross-correlation: 0.30 ± 0.09; Fig. 5; see Table S5 for details). The local-iFC patterns were also spatially well correlated with the local-iFC patterns of the original sample (mean coefficient: 0.49 ± 0.08; Fig. 6 and Table S5). Finally, the iFC peaks were located less than or equal to 6 voxels in the Y-Z plane, irrespective of the side, in more than half of them (those corresponding to IC15, IC11, IC3, IC1, IC10, IC8, and IC18 of the original sample).

For the replication sample 2 (N = 29; Figs. 5 and 6), nine independent components were identified as 'neural.' Of these 9, four had highest spatial cross-correlations with the original sample's global-iFC patterns: one global-iFC pattern had the highest spatial cross-correlation with the original orbitofrontal iFC pattern; one had it with the original frontoinsular and thalamus/basal ganglia; one with the original anterior cingulate, brain stem, left ventral, and dorsal frontal and parietal; and one with the five remaining original global-iFC patterns, all of which resembled subparts of the default mode network (mean coefficient: 0.25 ± 0.08; Fig. 5, Table S6). The corresponding local-iFC patterns were also spatially correlated with the original local-iFC patterns (mean coefficient: 0.43 ± 0.13; Fig. 6 and Table S6). Finally, as with the first replication sample, more than half of all iFC peaks were located less than or equal to 6 voxels in the Y-Z plane (the same as those of the first replication sample except for IC11 and with IC2 and IC9 in addition).

3.4.2. The particular role of the amygdala in the A-MTL global-iFC patterns

The longitudinal organization of the ("core") MTL and its whole-brain connectivity has been described already (e.g., Kahn et al., 2008). Therefore, given that we are studying the more comprehensive A-MTL, the particular contribution of the amygdala to the known core-MTL global-iFC should be specified. Thus, to appreciate in more detail the particular, additional contribution of the amygdala to the A-MTL

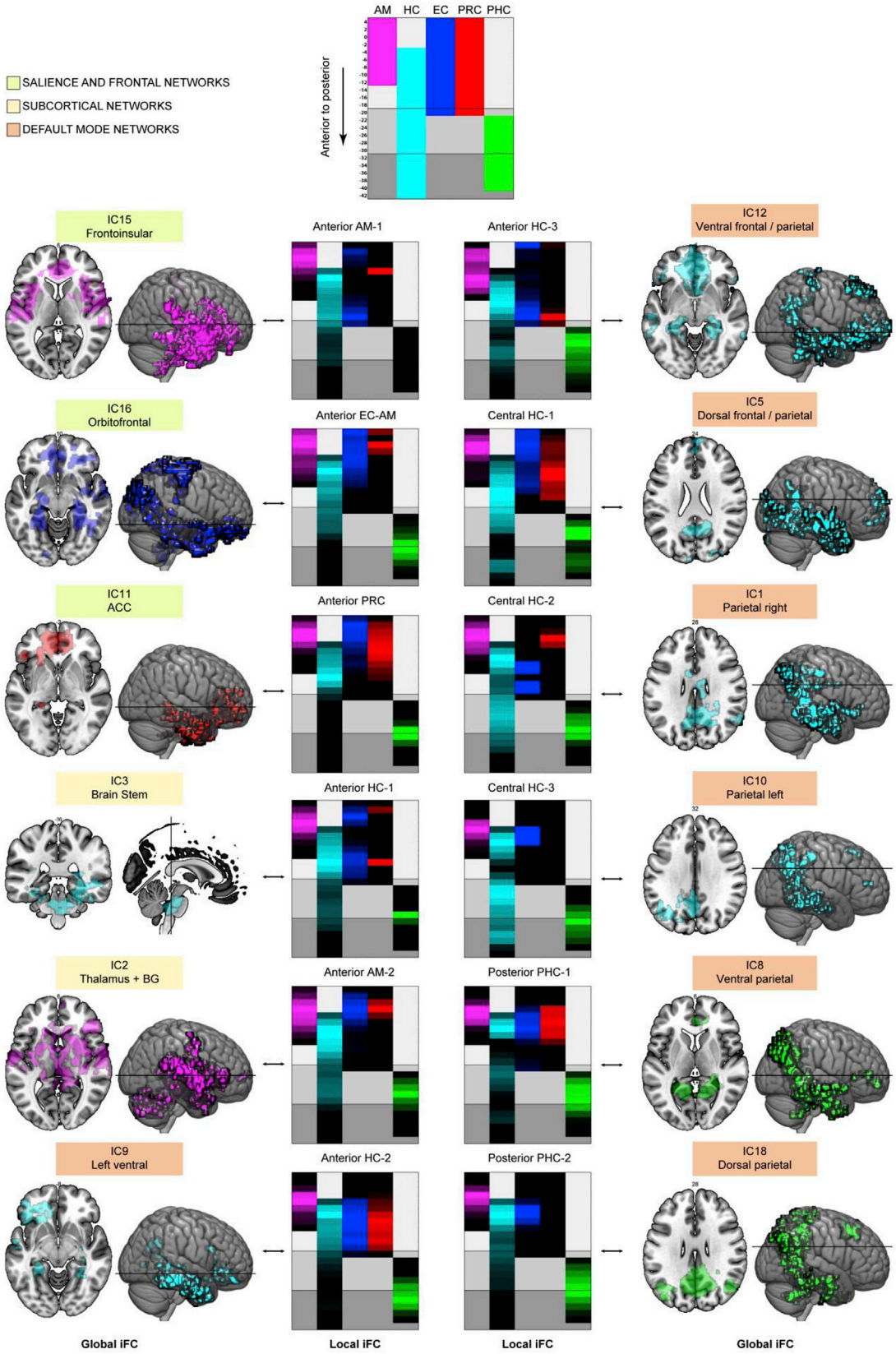

Fig. 4. Schematics of local-iFC patterns and their corresponding global-iFC patterns. Each local-iFC pattern of Fig. 3 is schematically represented slice by slice for each A-MTL structure, based on the number of voxels of the pattern falling on that structure and that slice (center). Coronal slices and brain renders show the extension of global-iFC patterns (outer columns). Shades of gray in the schematics demarcate anterior, middle, and posterior A-MTL according to Kivisaari et al. (2013). ACC = Anterior cingulate cortex; BG = basal ganglia; FWE = family wise error; IC = independent component; L = left; R = right.

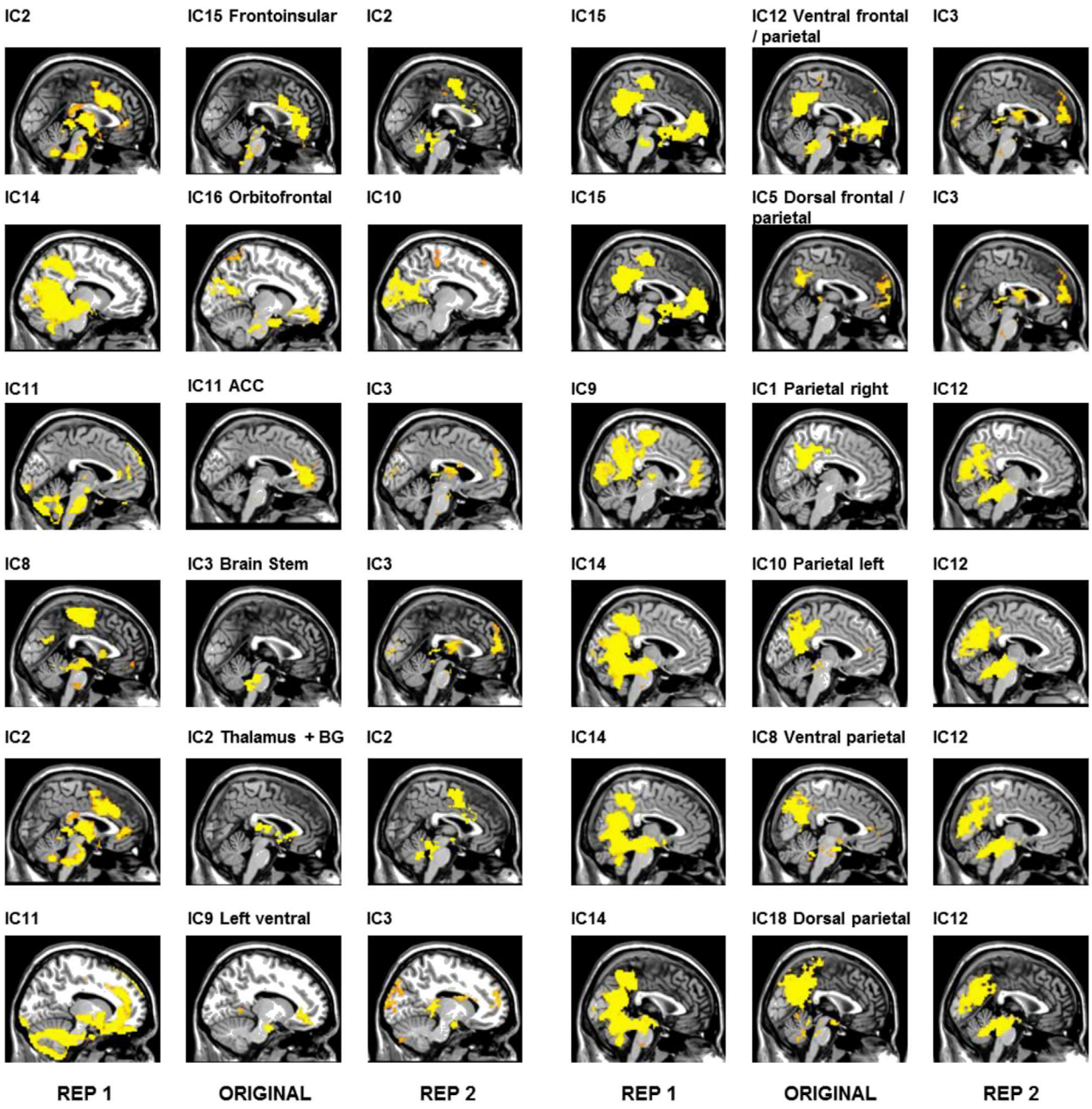

Fig. 5. Replication of global-iFC patterns. Sagittal view of the global-iFC patterns obtained from masked independent component analysis (mICA) restricted to the medial temporal lobe including the amygdala (A-MTL) in three different samples of cognitively normal adults (middle column: original sample; first column: replication sample 1, REP 1; third column: replication sample 2, REP 2).

global-iFC patterns, we extracted the time courses of (a) a region of interest corresponding to the amygdala and (b) a region of interest corresponding to the remaining regions ('core MTL'). Both regions of interest were based on the masks used for the mICA (see Supplementary Material for more information). We then correlated, separately, each of these time courses to those of the global-iFC patterns across data sets while controlling for the other. The results, depicted in Fig. 7, clearly indicate that the amygdala (A) largely contributed to the "salience and frontal networks" group, independently of the contribution of the remaining A-MTL regions, as the partial correlations were significantly positive ($p < 0.05$, FDR corrected, $q < 0.05$). The partial correlations with the next three global-iFC patterns (the two "subcortical networks" and the most anterior of the "default mode networks," see Fig. 4) were around zero, with that of the Thalamus + BG (IC2) being nonsignificant ((r transformed) Z-value = −0.011, p = 0.654). Finally, the partial correlations with the remaining global-iFC patterns were slightly negative (Z-values between −0.106 and −0.216). In contrast, the partial correlations of the remaining A-MTL structures, or 'core MTL' (B), showed almost the opposite picture: its largest contribution was to the global-iFC patterns corresponding to the "default mode networks," followed by those corresponding to "subcortical networks," and, finally, at the least, to the global-iFC patterns of the "salience and frontal networks" (see the simple correlations in Fig. S3).

3.4.3. *Impact of signal-to-noise ratio (SNR) and smoothing*

To account for the possible impact of magnetic susceptibility differences across A-MTL structures in our data, we calculated the temporal SNR (T-SNR). Both entorhinal and perirhinal cortices had lower T-SNR than the rest of the A-MTL structures (Fig. S5), and the entorhinal cortex had significantly lower T-SNR than the perirhinal cortex across participants (see Supplementary Material).

To assess the impact of spatial smoothing on the spatial specificity of

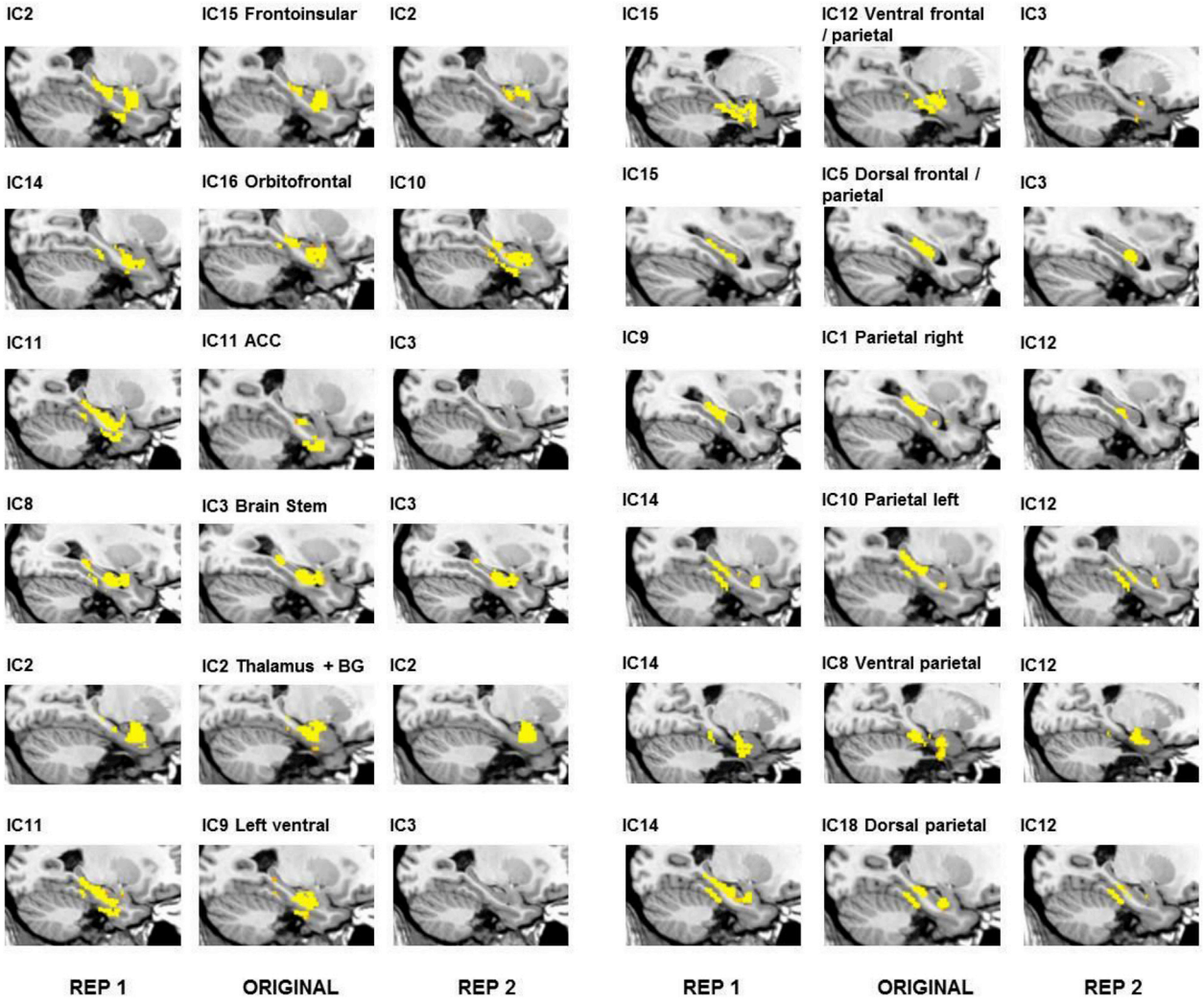

Fig. 6. Replication of local-iFC patterns. Sagittal view of the local-iFC patterns obtained from masked independent component analysis (mICA) restricted to the medial temporal lobe and amygdala (A-MTL) in three different samples of cognitively normal young adults (middle column: original sample; first column: replication sample 1, REP 1; third column: replication sample 2, REP 2).

our local-iFC results, we conducted additional mICA on unsmoothed data. Smoothing did not change the particular contribution of the amygdala or core MTL to the A-MTL global-iFC patterns (Fig. S4). Similarly, the structure-specific effect sizes remained similar between smoothed and unsmoothed data (Figs. S6 and S7), with the most noticeable difference concerning the perirhinal and entorhinal cortices, which no longer appear as the 'highest' in the neural patterns but only in the non-neural patterns instead (see Supplementary Material). Finally, smoothed and unsmoothed data did not differ in the percentage of involvement (i.e., percentage of voxels included in the pattern relative to each structure's size) of any A-MTL structure, independently of whether or not the local-iFC patterns had been classified as neural (Figs. S8 and S9).

4. Discussion

Using a data-driven approach on rs-fMRI data of healthy adults, we identified twelve intrinsic functional connectivity-based subsystems spanning the amygdala and the MTL (A-MTL) with two fundamental properties. First, all subsystems consistently covered parts of the amygdala, the hippocampus, and the entorhinal cortex. Second, subsystems showed a discrete organization along the longitudinal axis of the medial temporal lobes. The distinctive anterior-posterior organization of local connectivity at the A-MTL level is mirrored by a corresponding longitudinal arrangement at the global connectivity level. Specifically, global intrinsic connectivity patterns of A-MTL subsystems are arranged from prefrontal-insular, through subcortical, to posterior cingulate centered patterns. These patterns were remarkably similar to known large-scale brain networks, which are associated with distinct functional domains, proposed to support allostatic-interoceptive functions (Kleckner et al., 2017). These networks were the salience, basal ganglia/thalamus, hypothalamus/brainstem, and default mode networks. Thus, our results provide empirical evidence in humans for distinct A-MTL intrinsic connectivity subsystems with both (i) consistent recruitment of the amygdala, hippocampus, and entorhinal cortex, and (ii) a longitudinal anterior-posterior gradient that corresponds with global-iFC patterns of overlapping insular-cingulate and subcortically centered large-scale brain networks.

4.1. A-MTL subsystems derived from A-MTL local- and global-iFC patterns

4.1.1. A-MTL subsystems include the amygdala, the hippocampus, and the entorhinal cortex, and extend along the A-MTL longitudinal axis

One of our primary results is that A-MTL local-iFC patterns consistently span parts of both amygdala and core MTL regions, namely, hippocampus and entorhinal cortex (Fig. 4). Importantly, these local-iFC

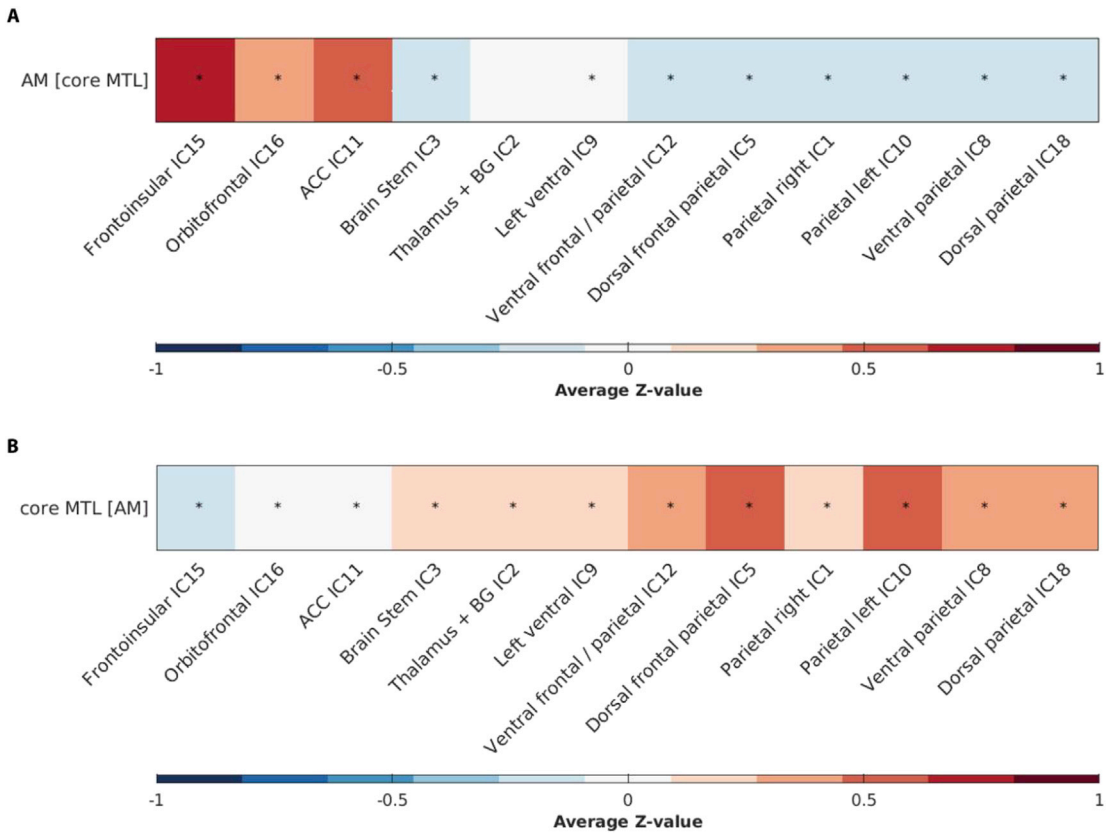

Fig. 7. Particular contribution of the amygdala to the A-MTL global-iFC patterns. Average correlations (r-to-Z transformed) between the time courses of the amygdala (AM) and the global-iFC patterns while controlling for the time course of the remaining A-MTL regions ('core MTL') (A). Average correlations (r-to-Z transformed) between the time courses of the core MTL and global-iFC patterns while controlling for the time course of the AM. Stars show significant correlations ($p < 0.05$) controlling for false discovery rate (FDR), $q < 0.05$.

patterns were independent both from methodological aspects such as mICA dimensionality (Fig. S1; Table S2), and sample properties (Fig. 6; Tables S5 and S6), thus underscoring the reliability of this finding. Such a combined contribution of the hippocampus and the entorhinal cortex is consistent with the cortical connectivity of the core MTL, with common input into the entorhinal cortex, intra-hippocampal loops, and output via entorhinal cortex (see, e.g., Burwell, 2000; Buzsaki, 2011). Our result is also in line with the previously shown convergence of functional connectivity of both regions, both within and outside the A-MTL, in human neuroimaging studies. For example, anterior parts of both the hippocampus and the entorhinal cortex have been shown to be functionally connected with the lateral temporal cortex (Kahn et al., 2008). Organized functional connectivity has moreover been shown between sub-regions of the entorhinal cortex and the hippocampus on the one hand, and the perirhinal/parahippocampal cortices on the other (Maass et al., 2015). Functional connectivity of the hippocampus, in turn, also extends to the amygdala, in particular to basolateral portions (Roy et al., 2009). Importantly, organized connectivity among the hippocampus, entorhinal cortex, and amygdala is also supported by evidence from structural connectivity, and anatomical, molecular, and functional studies in rodents and primates (Pitkanen et al., 2000; Swanson, 2003; Canto et al., 2008; Strange et al., 2014). For example, reviewed data of connectivity in rodents show substantial reciprocal interconnections between the lateral, basal, and accessory basal nuclei of the amygdala, and the rostral entorhinal cortex and temporal end of the hippocampus (Pitkanen et al., 2000). Functionally, the three structures show an integrated, sequential role in memory consolidation and retrieval (Izquierdo and Medina, 1993; Izquierdo et al., 1997) as well as coordinated activity and plasticity (Yaniv et al., 2003). For example, retrograde amnesia has been shown in rats after infusion of a $GABA_A$ receptor agonist or a glutamate AMPA receptor antagonist, given immediately (but not at 30 min) post-training into the hippocampus and amygdala, and at 30–180 min (but not immediately) into the entorhinal cortex (Izquierdo et al., 1997).

The identified A-MTL subsystems could be further differentiated by their iFC peak (Fig. 2A). These peaks were located in distinct structures of the A-MTL along its longitudinal axis (Fig. 3), which corresponded to the effect size of the involvement of each A-MTL structure in each iFC pattern (Fig. 2B) and were, to a large extent (i.e., for the majority of A-MTL subsystems), replicated in two additional, non-overlapping samples (Figs. 5 and 6; Tables S5 and S6). We interpret this finding as evidence for a distinctive anterior-posterior organization of subsystems in the A-MTL, with the peak location acting as each subsystem's functional 'anchor.' The results based on this data-driven approach are in line with previous neuroimaging reports of distinctive functional organization among core MTL structures (Kahn et al., 2008; Libby et al., 2012; Maass et al., 2015) or amygdala sub-regions (Roy et al., 2009) in humans. Crucially, our results extend those reports by revealing a discrete yet integrative functional organization of the core MTL and amygdala structures (Fig. 7). Our results also expand to the entire A-MTL previous data-driven findings reporting discrete functional sub-regions along the human hippocampus (Blessing et al., 2016). Furthermore, our longitudinally arranged A-MTL subsystems also match the longitudinally organized core MTL subsystems described in rodents and non-human primates as defined by other methods (for particular examples, see, e.g, Strange et al., 2014). Detailed comparative studies should, however, determine whether A-MTL subsystems obtained from functional connectivity in humans overlap with genetically or anatomically defined A-MTL subsystems in animal models.

4.1.2. Global cortical and subcortical connectivity patterns mirror the local organization of the A-MTL

The twelve A-MTL subsystems we found are embedded into global-iFC patterns that follow, at a cortico-subcortical level, the longitudinal A-MTL organization (Fig. 4). Previous research has already shown that the anterior-posterior organization within the MTL is differentially associated with global-iFC patterns (e.g., Ranganath and Ritchey, 2012; Wang et al., 2016). However, our results extend this knowledge by showing that the longitudinal organization of the 'core' MTL also includes the amygdala, thereby providing evidence for a 'small-scale' framework that integrates apparently disparate large-scale functional networks. In particular, global-iFC patterns are located in medial insular-cingulate and basal ganglia/thalamus/hypothalamus regions that overlap with medial cortical and subcortical brain networks: the default mode, salience, basal ganglia/thalamus, and hypothalamus/brainstem networks. These cortico-subcortical brain networks, associated with distinct functional domains, have been recently suggested to collectively modulate allostatic-interoceptive functions in humans (Barrett and Simmons, 2015; Kleckner et al., 2017). Next, we will describe these A-MTL subsystems and their embedding in the global-iFC patterns in more detail.

4.2. Single A-MTL subsystems and their embedding into global-iFC patterns

4.2.1. Anterior/frontoinsular A-MTL subsystems

The three anterior/frontoinsular A-MTL subsystems were centered on the amygdala, the anterior hippocampus, and the perirhinal cortex, and connected to the anterior and central hippocampus, and the entorhinal and parahippocampal cortices. At the global level, these subsystems included the anterior cingulate, orbitofrontal, and insular cortices; the putamen, ventral striatum, ventral pallidum, cerebellum, and periaqueductal gray; and the temporal pole. Note that the spatial resolution of our rs-fMRI data impeded a more reliable anatomical characterization at the level of the amygdala nuclei (see *Limitations*). Previous studies in humans have shown similar local and global patterns of connectivity for the perirhinal cortex (Kahn et al., 2008; Libby et al., 2012; Wang et al., 2016) and the amygdala (Roy et al., 2009), though separately. For example, the perirhinal cortex has been shown to exhibit preferential connectivity with the anterior hippocampus as well as with an anterior temporal and frontal cortical network (Libby et al., 2012). The amygdala, in turn, has shown organized functional connectivity between its basolateral division and the hippocampus, parahippocampal gyrus, and superior temporal gyrus; between its centromedial division and striatum, insula, cerebellum, and dorsal anterior cingulate cortex; and between its superficial division and the cingulate gyrus, hippocampus, caudate, and nucleus accumbens (Roy et al., 2009).

Previous structural connectivity evidence from animal studies (e.g., Van Hoesen and Pandya, 1975; Deacon et al., 1983; Carmichael and Price, 1995; McDonald et al., 1999; Stefanacci and Amaral, 2000) also supports our findings. For example, extensive reciprocal connections with the amygdala (e.g., medial and lateral, medial basal, accessory basal, and cortical nuclei) in the macaque have been shown for agranular and dysgranular insula (Mufson et al., 1981). Similar projections have also been shown for MTL regions such as the parahippocampal cortex, the superior temporal gyrus (Stefanacci and Amaral, 2000), the rostral entorhinal cortex, and – at a higher proportion – the rostral perirhinal cortex, which also receives back-projections from the amygdala (Deacon et al., 1983). Regions of the three anterior/frontoinsular A-MTL subsystems have previously been implied in semantically driven personal evaluations of social and asocial stimuli (Guo et al., 2013; Zhou and Seeley, 2014; Ranasinghe et al., 2016) as well as in emotional-autonomic responses, salience processing, and inhibitory control (Heimer and Van Hoesen, 2006; Seeley et al., 2007; Menon and Uddin, 2010), highly resembling a semantic-appraisal network and the aforementioned salience network, respectively.

4.2.2. Anterior/subcortical A-MTL subsystems

Anterior/subcortical A-MTL subsystems were centered on anterior portions of the hippocampus and showed connectivity to the amygdala, central hippocampus, and entorhinal, perirhinal, and parahippocampal cortices. These subsystems were also functionally connected to ventromedial frontal and insular cortices, superior temporal gyrus, basal forebrain, nucleus accumbens, caudate nucleus, putamen, thalamus, hypothalamus, and upper pons. Previous studies in humans have also reported specific connectivity of the anterior hippocampus to the hypothalamus (Blessing et al., 2016); prefrontal cortex (Zarei et al., 2013); caudate, putamen, and nucleus accumbens (Qin et al., 2015); entorhinal and perirhinal cortices (Kahn et al., 2008); and amygdala and insula (Robinson et al., 2015).

Neuronal connectivity evidence from rodents and primates has indicated a set of descending projections from ventral hippocampal/subicular, amygdalar, and medial prefrontal cortical structures to the periventricular and medial zones of the hypothalamus involved in neuroendocrine, autonomic, and motivated behavior (Fanselow and Dong, 2010). Moreover, the connectivity of the anterior hippocampus to the ventral striatum and the mesolimbic dopamine system confers a role to the A-MTL in goal-directed behavior (Pennartz et al., 2011; Strange et al., 2014). Regions of these anterior/subcortical A-MTL subsystems are involved in reward-motivated behavior (Haber and Knutson, 2010), pain modulation (Zambreanu et al., 2005; Tracey and Mantyh, 2007), and complex motor and non-motor behavior (DeLong and Wichmann, 2007; Haber and Calzavara, 2009).

4.2.3. Posterior/default mode network A-MTL subsystems

Posterior/default mode network A-MTL subsystems were anchored to portions of the anterior hippocampus, as well as the central hippocampus, and the posterior parahippocampal cortex. These subsystems connected to the amygdala, the whole extension of the hippocampus, and entorhinal, perirhinal, and parahippocampal cortices. Additionally, these subsystems were functionally connected to ventromedial, and dorsomedial frontal cortices, subgenual anterior and posterior cingulate cortices, middle temporal gyrus, retrosplenial cortex, inferior parietal lobule, precuneus, occipital cortex, nucleus accumbens, hypothalamus, cerebellum, and lower brain stem. This organization confirms previous reports in other studies in humans (Kahn et al., 2008; Libby et al., 2012; Qin et al., 2015; Wang et al., 2016). For example, the connectivity with the default mode network along the parahippocampal gyrus is characterized by being dominantly posterior (Qin et al., 2015). In other words, compared to its anterior portions (i.e., perirhinal cortex), the posterior portions of the parahippocampal gyrus (i.e., parahippocampal cortex) show stronger connectivity with default mode regions – such as the posterior cingulate cortex, retrosplenial cortex, or inferior temporal gyrus – (Wang et al., 2016). Middle and posterior parts of the hippocampus show a similar posterior-predominant pattern with posterior cingulate cortex (Zarei et al., 2013; Wang et al., 2016), whereas anterior parts of the hippocampus show this predominance with the prefrontal cortex (Zarei et al., 2013).

In humans, there is evidence of structural connectivity between the core MTL and the posterior component of the default mode network (i.e., the retrosplenial cortex) (Greicius et al., 2009). Similarly, the rostrocaudal topography of hippocampal projections compiled across primate studies indicates that projections to retrosplenial, anterior cingulate, or inferior temporal cortices arise, predominantly, from caudal (or posterior) portions of the hippocampus (Aggleton, 2012). Regions of the identified posterior/default mode networks and their interaction with the MTL have been associated, in general, with cognitive processes such as spatial navigation, planning, and semantic and episodic memory (Buckner et al., 2008).

4.3. Functional implications

Our findings indicate a functional organization for the whole MTL

that goes beyond previous proposals by showing the critical involvement of the amygdala in all A-MTL subsystems at the local level and its particular contribution to the salience and frontal networks at the global level. Moreover, the connectivity peaks found with our data-driven mICA approach highlight a longitudinal organization along the A-MTL that can further provide exact seed locations to inform future studies based on, e.g., structural MRI.

Beyond such local integration within the A-MTL, our results could complement – at large-scale systems level – the framework of a recently proposed 'allostatic-interoceptive system' (Barrett and Simmons, 2015; Kleckner et al., 2017). The allostatic-interoceptive system has been described as a domain-general brain system that includes visceromotor limbic – such as the cingulate cortices, ventral anterior insula, posterior orbitofrontal cortex, temporal pole, and parahippocampal gyrus – and primary interoceptive cortices – like the mid and posterior insula – as well as subcortical structures – like striatum and hypothalamus – (Barrett and Simmons, 2015; Chanes and Barrett, 2016). These regions correspond to exactly the same cortical and subcortical A-MTL subsystems described in the present study: the 'anterior/frontoinsular,' the 'anterior/subcortical,' and the 'posterior/default mode network' A-MTL subsystems. From a functional perspective, the allostatic-interoceptive system has been proposed to underpin functions that link the control of homeostatic body-oriented processes (i.e., interoception) with the body-referenced control of behavioral interactions of the organism with the environment (i.e., allostasis). In brief, the allostatic-interoceptive system matches the body's physiology with its behavior. Such system might constitute a unifying neural model integrating 'standard,' dichotomous views of core-MTL and amygdala functions (e.g., spatial navigation/memory consolidation and biological significance/emotional processing, respectively) but also more general psychological phenomena (e.g., decision making, novelty processing, or pain).

4.4. Limitations

In interpreting our results, several limitations must be taken into account. First, the spatial resolution used in our study prevented a solid outline of the sub-regional involvement within the A-MTL. This issue is especially nontrivial for structures with low signal-to-noise ratio like the entorhinal and perirhinal cortices, for which spatial smoothing was necessary to minimize signal loss. Of note, though, the current study was a first attempt at characterizing subsystems of the whole A-MTL and determining whether these subsystems cover both amygdala and core MTL regions alike. Moreover, control analyses support the reliability of the present findings by revealing good replicability across different samples and little influence from spatial smoothing. Second, the age variability across the cohorts we used to test the reliability of our results calls for caution in interpreting the present findings, given potential, age-relevant volumetric differences in the amygdala. Although the original sample did not differ from the second replication sample in the amygdala volume (post-hoc analysis), it did differ from that of the first replication sample (3.07 ± 0.30 vs 2.95 ± 0.28 cm^3, respectively, $p = 0.010$). Thus, age effects on A-MTL volume should be considered when examining A-MTL subsystems in a sample with large age variability. However, despite these volumetric (or MRI acquisition parameter) differences, A-MTL subsystems could be robustly reproduced in different samples. Acquisition parameter differences across samples (e.g., scanner type, spatial and temporal resolution, signal-to-noise ratio, or participants' demographics) should additionally be considered when interpreting our replication results (see Supplementary Material). Another limitation concerns the 'true' optimal dimensionality for the mICA. Given the characteristics of our data (sample size, repetition time, preprocessing, or number of volumes), we chose 20 components as an optimal solution and verified that we would obtain similar components if we used other dimensionalities. However, our results cannot be taken to show that 20 is the only dimensionality solution. Instead, the specific number might depend on the specific research question and the particular characteristics of the available data and should be compared to, at least, one other solution. Finally, assessing the impact of the global signal and its regression during preprocessing was outside the scope of this study. However, given the controversial nature of the global signal regression (e.g., Caballero-Gaudes and Reynolds, 2017; Power et al., 2017), future research could evaluate whether and how it particularly impacts mICA-based studies, especially when group comparisons, behavior, or arousal measures are involved (see, e.g., Turchi et al., 2018).

5. Conclusion

In summary, *in-vivo* data-driven intrinsic functional connectivity in humans revealed subsystems of the medial temporal lobe including the amygdala that could be reproduced in different samples of cognitively normal adults. These subsystems consistently covered parts of the amygdala, hippocampus, and entorhinal cortex, and showed a discrete longitudinal organization along the medial temporal lobes. This distinctive anterior-posterior organization was also found at the level of the whole brain, with local subsystems being functionally connected to frontoinsular, subcortical, or default mode networks.

Disclosure statement

The authors declare no competing financial interests.

Declaration of competing interest

The authors declare no competing conflict of interests.

Acknowledgments

This work was supported by the European Union FP7 Marie Curie ITN Grant 606901 (INDIREA) and the German Academic Foundation. We thank Dr. Mihai Avram for providing the preprocessed data of the first replication sample.

Appendix A. Supplementary data

Supplementary data to this article can be found online at https://doi.org/10.1016/j.neuroimage.2019.116404.

References

Aggleton, J.P., 2012. Multiple anatomical systems embedded within the primate medial temporal lobe: implications for hippocampal function. Neurosci. Biobehav. Rev. 36 (7), 1579–1596. https://doi.org/10.1016/j.neubiorev.2011.09.005.

Allen, E.A., Erhardt, E.B., Damaraju, E., Gruner, W., Segall, J.M., Silva, R.F., et al., 2011. A baseline for the multivariate comparison of resting-state networks. Front. Syst. Neurosci. 5, 2. https://doi.org/10.3389/fnsys.2011.00002.

Amaral, D.G., Insausti, R., 1992. Retrograde transport of D-[3H]-aspartate injected into the monkey amygdaloid complex. Exp. Brain Res. 88 (2), 375–388.

Amunts, K., Kedo, O., Kindler, M., Pieperhoff, P., Mohlberg, H., Shah, N.J., et al., 2005. Cytoarchitectonic mapping of the human amygdala, hippocampal region and entorhinal cortex: intersubject variability and probability maps. Anat. Embryol. 210 (5–6), 343–352. https://doi.org/10.1007/s00429-005-0025-5.

Barrett, L.F., Simmons, W.K., 2015. Interoceptive predictions in the brain. Nat. Rev. Neurosci. 16 (7), 419–429. https://doi.org/10.1038/nrn3950.

Beckmann, C.F., Mackay, C.E., Filippini, N., Smith, S., 2009. Group comparison of resting-state FMRI data using multi-subject ICA and dual regression. Neuroimage 47 (Suppl. 1), S148.

Beckmann, C.F., Smith, S.M., 2004. Probabilistic independent component analysis for functional magnetic resonance imaging. IEEE Trans. Med. Imaging 23 (2), 137–152. https://doi.org/10.1109/TMI.2003.822821.

Beissner, F., Schumann, A., Brunn, F., Eisentrager, D., Bar, K.J., 2014. Advances in functional magnetic resonance imaging of the human brainstem. Neuroimage 86, 91–98. https://doi.org/10.1016/j.neuroimage.2013.07.081.

Blackford, J.U., Buckholtz, J.W., Avery, S.N., Zald, D.H., 2010. A unique role for the human amygdala in novelty detection. Neuroimage 50 (3), 1188–1193. https://doi.org/10.1016/j.neuroimage.2009.12.083.

Blaiotta, C., Freund, P., Cardoso, M.J., Ashburner, J., 2018. Generative diffeomorphic modelling of large MRI data sets for probabilistic template construction. Neuroimage 166, 117–134. https://doi.org/10.1016/j.neuroimage.2017.10.060.

Blessing, E.M., Beissner, F., Schumann, A., Brunner, F., Bar, K.J., 2016. A data-driven approach to mapping cortical and subcortical intrinsic functional connectivity along the longitudinal hippocampal axis. Hum. Brain Mapp. 37 (2), 462–476. https://doi.org/10.1002/hbm.23042.

Buckner, R.L., Andrews-Hanna, J.R., Schacter, D.L., 2008. The brain's default network: anatomy, function, and relevance to disease. Ann. N. Y. Acad. Sci. 1124, 1–38. https://doi.org/10.1196/annals.1440.011.

Burwell, R.D., 2000. The parahippocampal region: corticocortical connectivity. Ann. N. Y. Acad. Sci. 911, 25–42.

Buzsaki, G., 2011. Hippocampus. Scholarpedia 6 (1). (Accessed 26 January 2018).

Buzsaki, G., Moser, E.I., 2013. Memory, navigation and theta rhythm in the hippocampal-entorhinal system. Nat. Neurosci. 16 (2), 130–138. https://doi.org/10.1038/nn.3304.

Caballero-Gaudes, C., Reynolds, R.C., 2017. Methods for cleaning the BOLD fMRI signal. Neuroimage 154, 128–149. https://doi.org/10.1016/j.neuroimage.2016.12.018.

Canto, C.B., Wouterlood, F.G., Witter, M.P., 2008. What does the anatomical organization of the entorhinal cortex tell us? Neural Plast. 2008, 381243. https://doi.org/10.1155/2008/381243.

Carmichael, S.T., Price, J.L., 1995. Limbic connections of the orbital and medial prefrontal cortex in macaque monkeys. J. Comp. Neurol. 363 (4), 615–641. https://doi.org/10.1002/cne.903630408.

Chanes, L., Barrett, L.F., 2016. Redefining the role of limbic areas in cortical processing. Trends Cogn. Sci. 20 (2), 96–106. https://doi.org/10.1016/j.tics.2015.11.005.

Chao-Gan, Y., Yu-Feng, Z., 2010. DPARSF: a MATLAB toolbox for "pipeline" data analysis of resting-state fMRI. Front. Syst. Neurosci. 4, 13. https://doi.org/10.3389/fnsys.2010.00013.

Dantzer, R., O'Connor, J.C., Freund, G.G., Johnson, R.W., Kelley, K.W., 2008. From inflammation to sickness and depression: when the immune system subjugates the brain. Nat. Rev. Neurosci. 9 (1), 46–56. https://doi.org/10.1038/nrn2297.

Davis, M., 1992. The role of the amygdala in fear and anxiety. Annu. Rev. Neurosci. 15, 353–375. https://doi.org/10.1146/annurev.ne.15.030192.002033.

Davis, M., Rainnie, D., Cassell, M., 1994. Neurotransmission in the rat amygdala related to fear and anxiety. Trends Neurosci. 17 (5), 208–214.

Deacon, T.W., Eichenbaum, H., Rosenberg, P., Eckmann, K.W., 1983. Afferent connections of the perirhinal cortex in the rat. J. Comp. Neurol. 220 (2), 168–190. https://doi.org/10.1002/cne.902200205.

DeLong, M.R., Wichmann, T., 2007. Circuits and circuit disorders of the basal ganglia. Arch. Neurol. 64 (1), 20–24. https://doi.org/10.1001/archneur.64.1.20.

Dolcos, F., LaBar, K.S., Cabeza, R., 2004. Interaction between the amygdala and the medial temporal lobe memory system predicts better memory for emotional events. Neuron 42 (5), 855–863.

Etkin, A., Prater, K.E., Schatzberg, A.F., Menon, V., Greicius, M.D., 2009. Disrupted amygdalar subregion functional connectivity and evidence of a compensatory network in generalized anxiety disorder. Arch. Gen. Psychiatr. 66 (12), 1361–1372. https://doi.org/10.1001/archgenpsychiatry.2009.104.

Fanselow, M.S., Dong, H.W., 2010. Are the dorsal and ventral hippocampus functionally distinct structures? Neuron 65 (1), 7–19. https://doi.org/10.1016/j.neuron.2009.11.031.

Filippini, N., MacIntosh, B.J., Hough, M.G., Goodwin, G.M., Frisoni, G.B., Smith, S.M., et al., 2009. Distinct patterns of brain activity in young carriers of the APOE-epsilon4 allele. Proc. Natl. Acad. Sci. U. S. A. 106 (17), 7209–7214. https://doi.org/10.1073/pnas.0811879106.

Fox, A.S., Oler, J.A., Tromp do, P.M., Fudge, J.L., Kalin, N.H., 2015. Extending the amygdala in theories of threat processing. Trends Neurosci. 38 (5), 319–329. https://doi.org/10.1016/j.tins.2015.03.002.

Fox, M.D., Raichle, M.E., 2007. Spontaneous fluctuations in brain activity observed with functional magnetic resonance imaging. Nat. Rev. Neurosci. 8 (9), 700–711. https://doi.org/10.1038/nrn2201.

Greicius, M.D., Supekar, K., Menon, V., Dougherty, R.F., 2009. Resting-state functional connectivity reflects structural connectivity in the default mode network. Cerebr. Cortex 19 (1), 72–78. https://doi.org/10.1093/cercor/bhn059.

Gross, C.T., Canteras, N.S., 2012. The many paths to fear. Nat. Rev. Neurosci. 13 (9), 651–658. https://doi.org/10.1038/nrn3301.

Guo, C.C., Gorno-Tempini, M.L., Gesierich, B., Henry, M., Trujillo, A., Shany-Ur, T., et al., 2013. Anterior temporal lobe degeneration produces widespread network-driven dysfunction. Brain 136 (Pt 10), 2979–2991. https://doi.org/10.1093/brain/awt222.

Haber, S.N., Calzavara, R., 2009. The cortico-basal ganglia integrative network: the role of the thalamus. Brain Res. Bull. 78 (2–3), 69–74. https://doi.org/10.1016/j.brainresbull.2008.09.013.

Haber, S.N., Knutson, B., 2010. The reward circuit: linking primate anatomy and human imaging. Neuropsychopharmacology 35 (1), 4–26. https://doi.org/10.1038/npp.2009.129.

Heimer, L., Van Hoesen, G.W., 2006. The limbic lobe and its output channels: implications for emotional functions and adaptive behavior. Neurosci. Biobehav. Rev. 30 (2), 126–147. https://doi.org/10.1016/j.neubiorev.2005.06.006.

Hyvarinen, A., 1999. Fast and robust fixed-point algorithms for independent component analysis. IEEE Trans. Neural Netw. 10 (3), 626–634. https://doi.org/10.1109/72.761722.

Insausti, R., 1993. Comparative anatomy of the entorhinal cortex and hippocampus in mammals. *Hippocampus* 3 Spec No 19–26.

Izquierdo, I., Medina, J.H., 1993. Role of the amygdala, hippocampus and entorhinal cortex in memory consolidation and expression. Braz. J. Med. Biol. Res. 26 (6), 573–589.

Izquierdo, I., Quillfeldt, J.A., Zanatta, M.S., Quevedo, J., Schaeffer, E., Schmitz, P.K., et al., 1997. Sequential role of hippocampus and amygdala, entorhinal cortex and parietal cortex in formation and retrieval of memory for inhibitory avoidance in rats. Eur. J. Neurosci. 9 (4), 786–793.

Jenkinson, M., Beckmann, C.F., Behrens, T.E.J., Woolrich, M.W., Smith, S.M., 2012. FSL. NeuroImage 62 (2), 782–790. https://doi.org/10.1016/j.neuroimage.2011.09.015.

Kahn, I., Andrews-Hanna, J.R., Vincent, J.L., Snyder, A.Z., Buckner, R.L., 2008. Distinct cortical anatomy linked to subregions of the medial temporal lobe revealed by intrinsic functional connectivity. J. Neurophysiol. 100 (1), 129–139. https://doi.org/10.1152/jn.00077.2008.

Kaplan, R., Horner, A.J., Bandettini, P.A., Doeller, C.F., Burgess, N., 2014. Human hippocampal processing of environmental novelty during spatial navigation. Hippocampus 24 (7), 740–750. https://doi.org/10.1002/hipo.22264.

Kemppainen, S., Jolkkonen, E., Pitkanen, A., 2002. Projections from the posterior cortical nucleus of the amygdala to the hippocampal formation and parahippocampal region in rat. Hippocampus 12 (6), 735–755. https://doi.org/10.1002/hipo.10020.

Kivisaari, S.L., Probst, A., Taylor, K.I., 2013. The perirhinal, entorhinal, and parahippocampal cortices and Hippocampus: an overview of functional anatomy and protocol for their segmentation in MR images. In: Ulmer, S.A., Jansen, O. (Eds.), fMRI - Basics and Clinical Applications. Springer-Verlag Berlin Heidelberg, Berlin Heidelberg.

Kleckner, I.R., Zhang, J., Touroutoglou, A., Chanes, L., Xia, C., Simmons, W.K., et al., 2017. Evidence for a large-scale brain system supporting allostasis and interoception in humans. Nat. Hum. Behav. 1 https://doi.org/10.1038/s41562-017-0069.

Lathe, R., 2001. Hormones and the hippocampus. J. Endocrinol. 169 (2), 205–231. https://doi.org/10.1677/joe.0.1690205.

Libby, L.A., Ekstrom, A.D., Ragland, J.D., Ranganath, C., 2012. Differential connectivity of perirhinal and parahippocampal cortices within human hippocampal subregions revealed by high-resolution functional imaging. J. Neurosci. 32 (19), 6550–6560. https://doi.org/10.1523/JNEUROSCI.3711-11.2012.

Maass, A., Berron, D., Libby, L.A., Ranganath, C., Duzel, E., 2015. Functional subregions of the human entorhinal cortex. Elife 4. https://doi.org/10.7554/eLife.06426.

McDonald, A.J., 1998. Cortical pathways to the mammalian amygdala. Prog. Neurobiol. 55 (3), 257–332.

McDonald, A.J., Shammah-Lagnado, S.J., Shi, C., Davis, M., 1999. Cortical afferents to the extended amygdala. Ann. N. Y. Acad. Sci. 877, 309–338.

Menon, V., Uddin, L.Q., 2010. Saliency, switching, attention and control: a network model of insula function. Brain Struct. Funct. 214 (5–6), 655–667. https://doi.org/10.1007/s00429-010-0262-0.

Mufson, E.J., Mesulam, M.M., Pandya, D.N., 1981. Insular interconnections with the amygdala in the rhesus monkey. Neuroscience 6 (7), 1231–1248.

Murray, E.A., Wise, S.P., 2004. What, if anything, is the medial temporal lobe, and how can the amygdala be part of it if there is no such thing? Neurobiol. Learn. Mem. 82 (3), 178–198. https://doi.org/10.1016/j.nlm.2004.05.005.

Navarro Schroder, T., Haak, K.V., Zaragoza Jimenez, N.I., Beckmann, C.F., Doeller, C.F., 2015. Functional topography of the human entorhinal cortex. Elife 4. https://doi.org/10.7554/eLife.06738.

Nickerson, L.D., Smith, S.M., Ongur, D., Beckmann, C.F., 2017. Using dual regression to investigate network shape and amplitude in functional connectivity analyses. Front. Neurosci. 11, 115. https://doi.org/10.3389/fnins.2017.00115.

Oler, J.A., Birn, R.M., Patriat, R., Fox, A.S., Shelton, S.E., Burghy, C.A., et al., 2012. Evidence for coordinated functional activity within the extended amygdala of non-human and human primates. Neuroimage 61 (4), 1059–1066. https://doi.org/10.1016/j.neuroimage.2012.03.045.

Pennartz, C.M., Ito, R., Verschure, P.F., Battaglia, F.P., Robbins, T.W., 2011. The hippocampal-striatal axis in learning, prediction and goal-directed behavior. Trends Neurosci. 34 (10), 548–559. https://doi.org/10.1016/j.tins.2011.08.001.

Petrovich, G.D., Canteras, N.S., Swanson, L.W., 2001. Combinatorial amygdalar inputs to hippocampal domains and hypothalamic behavior systems. Brain Res. Brain Res. Rev. 38 (1–2), 247–289.

Phelps, E.A., 2004. Human emotion and memory: interactions of the amygdala and hippocampal complex. Curr. Opin. Neurobiol. 14 (2), 198–202. https://doi.org/10.1016/j.conb.2004.03.015.

Pitkanen, A., Pikkarainen, M., Nurminen, N., Ylinen, A., 2000. Reciprocal connections between the amygdala and the hippocampal formation, perirhinal cortex, and postrhinal cortex in rat. A review. Ann. N. Y. Acad. Sci. 911, 369–391.

Power, J.D., Plitt, M., Laumann, T.O., Martin, A., 2017. Sources and implications of whole-brain fMRI signals in humans. Neuroimage 146, 609–625. https://doi.org/10.1016/j.neuroimage.2016.09.038.

Qin, S., Duan, X., Supekar, K., Chen, H., Chen, T., Menon, V., 2015. Large-scale intrinsic functional network organization along the long axis of the human medial temporal lobe. Brain Struct. Funct. https://doi.org/10.1007/s00429-015-1098-4.

Raichle, M.E., 2015. The Brain's Default Mode Network. Annual review of neuroscience 38, 433–447. https://doi.org/10.1146/annurev-neuro-071013-014030.

Ranasinghe, K.G., Rankin, K.P., Pressman, P.S., Perry, D.C., Lobach, I.V., Seeley, W.W., et al., 2016. Distinct subtypes of behavioral variant frontotemporal dementia based on patterns of network degeneration. JAMA Neurol. 73 (9), 1078–1088. https://doi.org/10.1001/jamaneurol.2016.2016.

Ranganath, C., Ritchey, M., 2012. Two cortical systems for memory-guided behaviour. Nat. Rev. Neurosci. 13 (10), 713–726. https://doi.org/10.1038/nrn3338.

Robinson, J.L., Barron, D.S., Kirby, L.A., Bottenhorn, K.L., Hill, A.C., Murphy, J.E., et al., 2015. Neurofunctional topography of the human hippocampus. Hum. Brain Mapp. https://doi.org/10.1002/hbm.22987.

Roy, A.K., Shehzad, Z., Margulies, D.S., Kelly, A.M., Uddin, L.Q., Gotimer, K., et al., 2009. Functional connectivity of the human amygdala using resting state fMRI. Neuroimage 45 (2), 614–626. https://doi.org/10.1016/j.neuroimage.2008.11.030.

Rutishauser, U., Mamelak, A.N., Schuman, E.M., 2006. Single-trial learning of novel stimuli by individual neurons of the human hippocampus-amygdala complex. Neuron 49 (6), 805–813. https://doi.org/10.1016/j.neuron.2006.02.015.

Sah, P., Faber, E.S., Lopez De Armentia, M., Power, J., 2003. The amygdaloid complex: anatomy and physiology. Physiol. Rev. 83 (3), 803–834. https://doi.org/10.1152/physrev.00002.2003.

Saunders, R.C., Rosene, D.L., 1988. A comparison of the efferents of the amygdala and the hippocampal formation in the rhesus monkey: I. Convergence in the entorhinal, prorhinal, and perirhinal cortices. J. Comp. Neurol. 271 (2), 153–184. https://doi.org/10.1002/cne.902710202.

Seeley, W.W., Menon, V., Schatzberg, A.F., Keller, J., Glover, G.H., Kenna, H., et al., 2007. Dissociable intrinsic connectivity networks for salience processing and executive control. J. Neurosci. 27 (9), 2349–2356. https://doi.org/10.1523/JNEUROSCI.5587-06.2007.

Sheth, A., Berretta, S., Lange, N., Eichenbaum, H., 2008. The amygdala modulates neuronal activation in the hippocampus in response to spatial novelty. Hippocampus 18 (2), 169–181. https://doi.org/10.1002/hipo.20380.

Smith, D.V., Utevsky, A.V., Bland, A.R., Clement, N., Clithero, J.A., Harsch, A.E., et al., 2014. Characterizing individual differences in functional connectivity using dual-regression and seed-based approaches. Neuroimage 95, 1–12. https://doi.org/10.1016/j.neuroimage.2014.03.042.

Smith, S.M., Fox, P.T., Miller, K.L., Glahn, D.C., Fox, P.M., Mackay, C.E., et al., 2009. Correspondence of the brain's functional architecture during activation and rest. Proc. Natl. Acad. Sci. U. S. A. 106 (31), 13040–13045. https://doi.org/10.1073/pnas.0905267106.

Smith, S.M., Nichols, T.E., 2009. Threshold-free cluster enhancement: addressing problems of smoothing, threshold dependence and localisation in cluster inference. Neuroimage 44 (1), 83–98. https://doi.org/10.1016/j.neuroimage.2008.03.061.

Squire, L.R., Stark, C.E., Clark, R.E., 2004. The medial temporal lobe. Annu. Rev. Neurosci. 27, 279–306. https://doi.org/10.1146/annurev.neuro.27.070203.144130.

Stefanacci, L., Amaral, D.G., 2000. Topographic organization of cortical inputs to the lateral nucleus of the macaque monkey amygdala: a retrograde tracing study. J. Comp. Neurol. 421 (1), 52–79.

Strange, B.A., Witter, M.P., Lein, E.S., Moser, E.I., 2014. Functional organization of the hippocampal longitudinal axis. Nat. Rev. Neurosci. 15 (10), 655–669. https://doi.org/10.1038/nrn3785.

Suarez, A.N., Hsu, T.M., Liu, C.M., Noble, E.E., Cortella, A.M., Nakamoto, E.M., et al., 2018. Gut vagal sensory signaling regulates hippocampus function through multi-order pathways. Nat. Commun. 9 (1), 2181. https://doi.org/10.1038/s41467-018-04639-1.

Swanson, L.W., 2003. The amygdala and its place in the cerebral hemisphere. Ann. N. Y. Acad. Sci. 985, 174–184.

Tovote, P., Fadok, J.P., Luthi, A., 2015. Neuronal circuits for fear and anxiety. Nat. Rev. Neurosci. 16 (6), 317–331. https://doi.org/10.1038/nrn3945.

Tracey, I., Mantyh, P.W., 2007. The cerebral signature for pain perception and its modulation. Neuron 55 (3), 377–391. https://doi.org/10.1016/j.neuron.2007.07.012.

Turchi, J., Chang, C., Ye, F.Q., Russ, B.E., Yu, D.K., Cortes, C.R., et al., 2018. The basal forebrain regulates global resting-state fMRI fluctuations. Neuron 97 (4), 940–952. https://doi.org/10.1016/j.neuron.2018.01.032 e944.

Van Hoesen, G., Pandya, D.N., 1975. Some connections of the entorhinal (area 28) and perirhinal (area 35) cortices of the rhesus monkey. I. Temporal lobe afferents. Brain Res. 95 (1), 1–24.

Van Hoesen, G.W., 1995. Anatomy of the medial temporal lobe. Magn. Reson. Imaging 13 (8), 1047–1055.

Wang, S.F., Ritchey, M., Libby, L.A., Ranganath, C., 2016. Functional connectivity based parcellation of the human medial temporal lobe. Neurobiol. Learn. Mem. 134 Pt A, 123–134. https://doi.org/10.1016/j.nlm.2016.01.005.

Yaniv, D., Vouimba, R.M., Diamond, D.M., Richter-Levin, G., 2003. Simultaneous induction of long-term potentiation in the hippocampus and the amygdala by entorhinal cortex activation: mechanistic and temporal profiles. Neuroscience 120 (4), 1125–1135.

Yeo, T.B.T., Krienen, F.M., Sepulcre, J., Sabuncu, M.R., Lashkari, D., Hollinshead, M., et al., 2011. The organization of the human cerebral cortex estimated by intrinsic functional connectivity. Journal of neurophysiology 106 (3), 1125–1165. https://doi.org/10.1152/jn.00338.2011.

Zambreanu, L., Wise, R.G., Brooks, J.C., Iannetti, G.D., Tracey, I., 2005. A role for the brainstem in central sensitisation in humans. Evidence from functional magnetic resonance imaging. Pain 114 (3), 397–407. https://doi.org/10.1016/j.pain.2005.01.005.

Zarei, M., Beckmann, C.F., Binnewijzend, M.A., Schoonheim, M.M., Oghabian, M.A., Sanz-Arigita, E.J., et al., 2013. Functional segmentation of the hippocampus in the healthy human brain and in Alzheimer's disease. Neuroimage 66, 28–35. https://doi.org/10.1016/j.neuroimage.2012.10.071.

Zhou, J., Seeley, W.W., 2014. Network dysfunction in Alzheimer's disease and frontotemporal dementia: implications for psychiatry. Biol. Psychiatry 75 (7), 565–573. https://doi.org/10.1016/j.biopsych.2014.01.020.